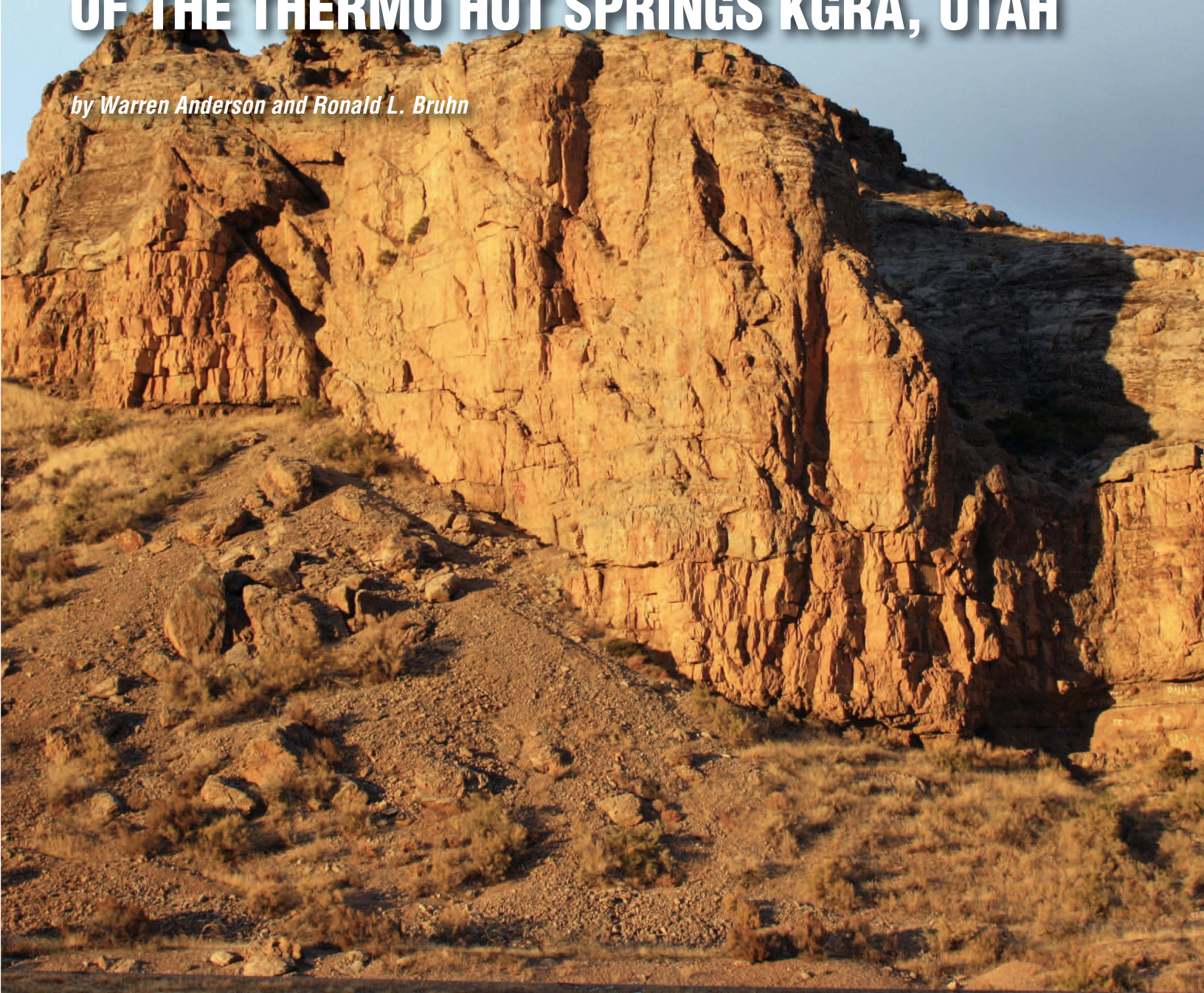


# IMPLICATIONS OF THRUST AND DETACHMENT FAULTING FOR THE STRUCTURAL GEOLOGY OF THE THERMO HOT SPRINGS KGRA, UTAH

*by Warren Anderson and Ronald L. Bruhn*



**OPEN-FILE REPORT 587**  
**UTAH GEOLOGICAL SURVEY**

*a division of*  
UTAH DEPARTMENT OF NATURAL RESOURCES  
**2012**

# Implications of Thrust and Detachment Faulting for the Structural Geology of the Thermo Hot Springs KGRA, Utah

Warren Anderson and Ronald L. Bruhn  
Department of Geology and Geophysics  
University of Utah  
115 S, 1460 E, Frederick A. Sutton Bldg., Rm. 383  
Contact email: [ron.bruhn@utah.edu](mailto:ron.bruhn@utah.edu)

*Cover photo: Outcrop of the Kaibab Formation, looking north towards the western edge of the southern Mineral Mountains, near Minersville, Utah.*



**OPEN-FILE REPORT 587**  
**UTAH GEOLOGICAL SURVEY**  
*a division of*  
**UTAH DEPARTMENT OF NATURAL RESOURCES**  
**2012**



**STATE OF UTAH**

Gary R. Herbert, Governor

**DEPARTMENT OF NATURAL RESOURCES**

Michael Styler, Executive Director

**UTAH GEOLOGICAL SURVEY**

Richard G. Allis, Director

**PUBLICATIONS**

contact

Natural Resources Map & Bookstore

1594 W. North Temple

Salt Lake City, UT 84114

telephone: 801-537-3320

toll-free: 1-888-UTAH MAP

website: [mapstore.utah.gov](http://mapstore.utah.gov)

email: [geostore@utah.gov](mailto:geostore@utah.gov)

**UTAH GEOLOGICAL SURVEY**

contact

1594 W. North Temple, Suite 3110

Salt Lake City, UT 84114

telephone: 801-537-3300

website: [geology.utah.gov](http://geology.utah.gov)

*This open-file release makes information available to the public that may not conform to UGS technical, editorial, or policy standards; this should be considered by an individual or group planning to take action based on the contents of this report. The Utah Department of Natural Resources, Utah Geological Survey, makes no warranty, expressed or implied, regarding its suitability for a particular use. The Utah Department of Natural Resources, Utah Geological Survey, shall not be liable under any circumstances for any direct, indirect, special, incidental, or consequential damages with respect to claims by users of this product.*

## CONTENTS

ABSTRACT.....	1
RESEARCH PROBLEM.....	1
RESEARCH METHODS AND PROCEDURES.....	2
GEOLOGICAL BACKGROUND.....	3
STRATIGRAPHY AND STRUCTURE OF RASERTECH WELL 17-34 .....	4
Overview of Subsurface Work.....	4
Stratigraphy.....	4
Structural Interpretation (7660–8770 ft).....	6
MINERAL MOUNTAINS ARE AN ANALOG TO THE KGRA RESERVOIR? .....	9
Stratigraphic and Structural Similarities.....	9
Detachment Faulting.....	9
Permeability Structure of Analog Outcrops.....	9
Locality 1: Low-angle normal fault near Corral Canyon.....	14
Locality 2: Faulting of Kaibab Formation and Queantoweap Sandstone .....	15
RAPID SPECTRAL DISCRIMINATION OF LITHOLOGY.....	16
Spectral Analysis of Chip Sample Boards.....	16
Spectral Analysis .....	16
IMPLICATIONS FOR GEOTHERMAL RESOURCES .....	17
CONCLUSIONS.....	21
ACKNOWLEDGMENTS .....	21
REFERENCES .....	22

## FIGURES

Figure 1. Satellite image of southwestern Utah showing the locations of the Thermo Hot Springs KGRA and southern Mineral Mountains study areas. ....	2
Figure 2. Geological map of the Thermo Hot Springs KGRA with locations of geothermal wells. ....	5
Figure 3. Stratigraphic column of well 17-34.....	7
Figure 4. Images of a petrographic thin section obtained from the sheared “skarn” deposit in the lower part of well 17-34. ....	8
Figure 5. The formation XRMI-scanner log data of well 17-34.....	10
Figure 6. Geologic map of the southern Mineral Mountains showing the formations and faults. ....	12
Figure 7. Geological cross section along line A-A' on the geological map in figure 6.....	14
Figure 8. Photographs showing the low-angle detachment fault near Corral Canyon on the western flank of the Mineral Mountains.....	14
Figure 9. Fracturing and faulting of the Kaibab Formation that illustrates how high-angle faulting affects the rock. ....	15
Figure 10. Brecciated Queantoweap Sandstone at the same locality as that shown in figure 9. ....	16
Figure 11. Example of a chip sample board for cuttings from borehole 17-34 and a board made by crushing a hand sample obtained from outcrop.....	17
Figure 12. Rock type discrimination plots showing results of comparing the spectra of chip samples at various depths in well 17-34 with those of standards obtained from samples of outcrops in the Mineral Mountains. ....	18



# Implications of Thrust and Detachment Faulting for the Structural Geology of the Thermo Hot Springs KGRA, Utah

*by Warren Anderson and Ronald L. Bruhn*

## ABSTRACT

This report presents data and conclusions concerning the role of low-angle faulting in the formation of the Thermo Hot Springs Known Geothermal Resource Area (KGRA) and the effects that such faulting may have on fluid flow and production. The conclusions are that the KGRA is formed by a low-angle normal or “detachment fault” that juxtaposes Mesozoic and upper Paleozoic sedimentary rock in the upper plate over underlying metamorphic rock and granite. The Mesozoic section is in turn overlain by a sequence of Tertiary to Quaternary volcanic and sedimentary deposits. High-angle normal faults offset the sedimentary and volcanic section, and in some, if not all, cases penetrate and offset the low-angle detachment fault. The high-angle normal faulting has two primary trends: one is the northern trend of classical Basin and Range faulting, and the other is a roughly east-west trending set of normal faults. These faults may hydraulically compartmentalize the reservoir but also provide pathways for fluids to ascend upwards from beneath the detachment fault. We find no evidence for duplication of the Paleozoic or Mesozoic section by either low-angle or ramp-style thrust faulting in the KGRA.

The implications of the low-angle normal or “detachment” fault structure are significant: (1) The Thermo Hot Springs KGRA has striking similarities to the structures and stratigraphy that are exposed in the southern Mineral Mountains, which provide an excellent outcrop analog for studying the nature of the structures and fluid conduits that presumably occur at depth in the KGRA. There is good reason to suspect that the Cave Canyon detachment fault exposed in the southern Mineral Mountains is the same or similar structure as the detachment fault within the Thermo Hot Springs KGRA. The similarities include lower fault plate granitic and metamorphic rocks, hydrothermally altered cataclasite within the detachment fault zone, essentially an identical stratigraphy within the upper plate of the detachment fault, and a mosaic of north and east trending high-angle normal faults, some of which penetrate and offset the detachment fault. (2) The low-angle detachment fault model for KGRA structure has regional implications for geothermal prospecting in the Basin and Range terrain of southwestern Utah. This region is underlain by several known or suspected detachment normal faults of middle to late Tertiary age, which may act to laterally channel hot fluids at depth over large areas with little surface expression except where the low-angle faults are breached by

younger faulting. That is, “blind” geothermal reservoirs may well occur at depth with few if any surface manifestations such as springs or tufa mounds. We suspect that thrust faults of Mesozoic age may also play a similar role to the Tertiary detachment faults in channeling fluids laterally in the Basin and Range region of southwestern Utah, but this is apparently not the case in the Thermo Hot Springs KGRA.

## RESEARCH PROBLEM

This research project is an initial investigation into the role that low-angle faulting may play in the structure and permeability of geothermal reservoirs within the Sevier geothermal anomaly of southwestern Utah. The work uses the Thermo Hot Springs KGRA as a case study (figure 1), but also has broader implications for exploration and development where stratigraphic sections were duplicated during Mesozoic thrusting, or alternatively, juxtaposed by subsequent extensional detachment faults. If low-angle faults, either Mesozoic thrust or alternatively, Cenozoic extensional detachment faults, control the structure and permeability of geothermal reservoirs the fluid volume and extractable energy of southwestern Utah geothermal systems may be significantly larger than usually thought. The presence of large bodies of hot fluid trapped beneath and/or channeled along low-angle fault planes may also enhance consideration of “high-risk” exploration schemes, where exploratory drilling is undertaken at sites without significant surface manifestation of upwelling fluid along high-angle faults.

The research consists of: (1) inspection of drill cuttings, thermal logs, and one available extended range micro-image (XRMI) scanner log for evidence of faulting at roughly similar stratigraphic position in the KGRA, and (2) inspection of stratigraphic sections and structures in analog outcrops from the central and southern Mineral Mountains for comparison with the lithology, deformation and alteration of drill hole samples and logging data. We compare our results with those of previous studies, and comment on further efforts to explore for “blind” geothermal resources. Our primary focus in this report is determining the stratigraphy and evidence for or against low-angle thrust and/or detachment faulting.

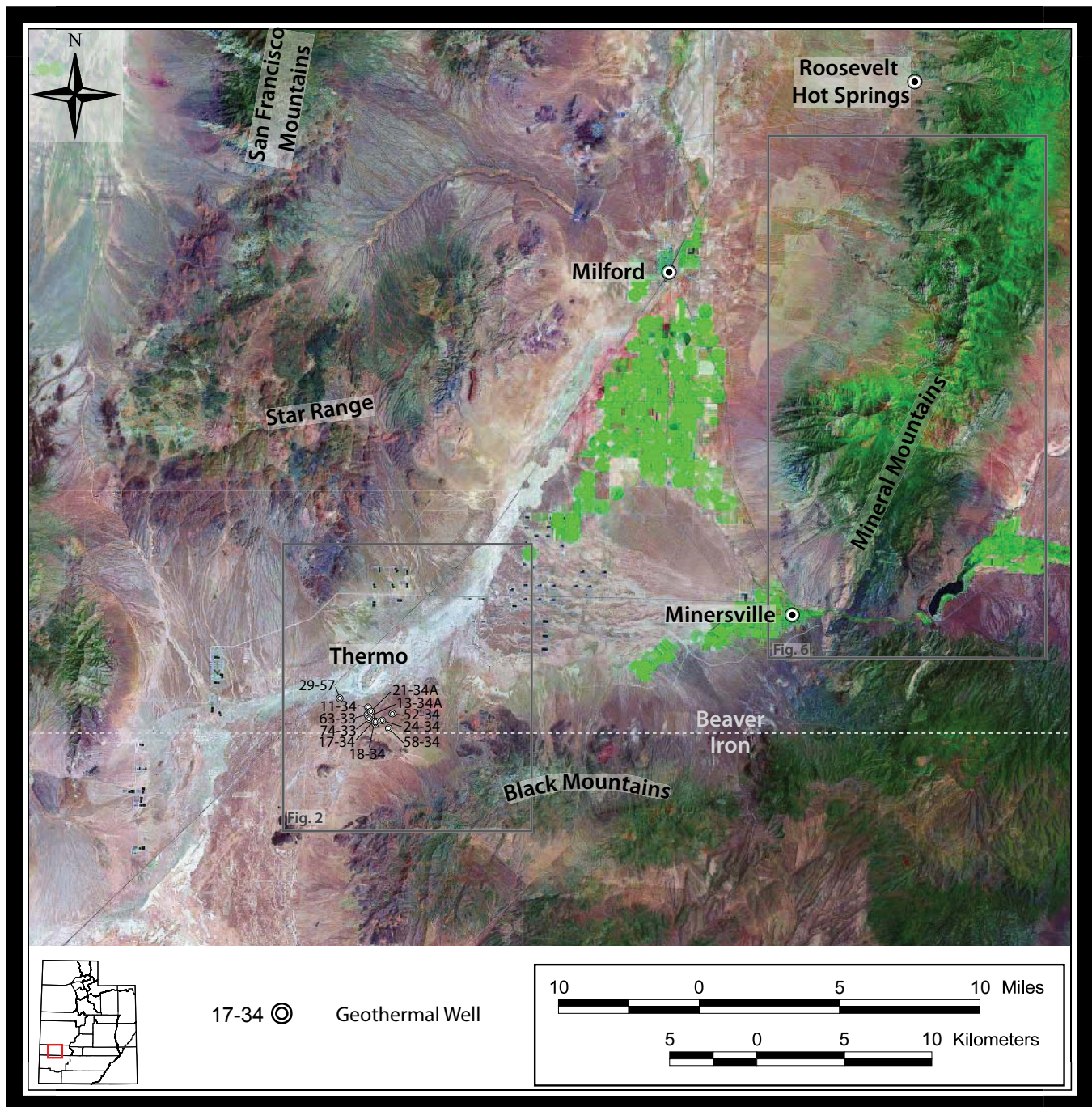


**Figure 1.** Satellite image of southwestern Utah showing the locations of the Thermo Hot Springs KGRA and southern Mineral Mountains study areas. Note that locations of maps shown in figures 2 and 6 are indicated by labeled rectangles.

## RESEARCH METHODS AND PROCEDURES

The research involved work in the laboratory and in the field.

- We completed a review of pertinent publications and reports concerning the Thermo Hot Springs KGRA and the geology of the surrounding terrain. We sought and received considerable advice and help from Dr. Joseph Moore at the Energy

and Geoscience Institute (EGI) at the University of Utah. Dr. Moore shared his knowledge of the Thermo Hot Springs KGRA, made available chip samples and thin sections, and provided copies of unpublished reports by Moore and others (2009) and Nash and Jones (2010) after obtaining permission from Raser Technologies, Inc. Mr. Clay Jones of EGI provided copies of geologic cross sections and information on well bore localities in the KGRA.



- Base maps for field mapping and analysis of the geomorphology were constructed using high-resolution digital aerial photographs and digital elevation models obtained from the online Utah Geographic Information System Portal. These data were used for mapping stratigraphy and structure in the southern Mineral Mountains, and for creating shaded relief images of the earth's surface that were inspected for evidence of faulting.
- Work in the field included approximately three weeks of effort. Bruhn and Anderson visited the site of the KGRA and the southern Mineral Mountains to become familiar with the geology, to collect rock samples of selected geologic formations and various metamorphic and igneous rocks, and to plan a field mapping campaign. Subsequently, Anderson and a field assistant spent approximately one week documenting and mapping geologic features in the southern Mineral Mountains as potential analogs to those in the subsurface of the KGRA. Additional rock samples were also collected and several panoramic images of cliff faces were obtained to facilitate mapping faults and joints at outcrop scale.
- Thirty-two rock samples of known age and map formation were collected from outcrops in the southern Mineral Mountains. Parts of these samples were crushed and mounted on chip sample boards. The analog sample boards were used to compare and correlate rocks of known age and type with board-mounted chip samples from well 17-34 in the KGRA.
- Petrographic thin sections were also prepared from the crushed outcrop samples and studied to determine the mineralogy. This work allowed us to directly compare the petrography of mapped rock units from the southern Mineral Mountains to thin sections of chip samples from the KGRA. About 70 thin sections from well 17-34 were studied in addition to the 32 thin sections of outcrop samples.
- Thin sections from the KGRA were inspected for fragments of fossils to constrain the age of the strata that were penetrated in the subsurface. This proved effective for assigning some samples to specific formations of upper Paleozoic and Mesozoic strata.
- An Analytical Spectral Device (ASD) spectrometer was used to collect the spectral properties of the chip samples from both the outcrop chip sample boards and from the KGRA borehole chip sample boards. Bruhn wrote a computer program that implemented the Spectral Angle Mapper (SAM) algorithm for rock and mineral discrimination. Spectra obtained from the outcrop chip

samples were compiled as a library of known rock units. Spectra obtained from borehole chip samples were then compared to the sample library using the SAM discrimination algorithm to facilitate correlation of rock types between the subsurface of the KGRA and the library samples of known rock type and formation or unit.

- A formation XRMI-scanner log from the lower part of well 17-34 was reviewed and the structural data plotted to reveal the distribution of structures within the KGRA reservoir, including fracturing and various dip domains of bedding and foliation.
- The field and laboratory data and analysis noted above were integrated with other published data on the geology and geophysics of the Thermo Hot Springs KGRA to evaluate the stratigraphy and structure of the geothermal system. In particular we tested and rejected the model where remnant thrust faults are present, and adopted an alternative model based on the presence of a low-angle normal "detachment fault" that may be part of the Cave Canyon detachment fault system in the southern Mineral Mountains.

## GEOLOGICAL BACKGROUND

The Sevier geothermal anomaly of southwestern Utah encompasses a broad region of enhanced heat flow with seven known high-temperature geothermal resource areas or "KGRA" (Mabey and Budding, 1987, 1994). The anomaly also encompasses the transition between the Colorado Plateau and the eastern Basin and Range Province, where the Paleozoic miogeocline was collapsed eastward by thrust faulting during the Cretaceous to early Tertiary Sevier orogeny, which also partially overlapped in space and time with the Laramide deformation in the Colorado Plateau and Rocky Mountains (Cowan and Bruhn, 1992). The subsequent history included widespread igneous activity, and extension that initiated during mid-Tertiary time and continues to the present. Thrust faults are exposed throughout mountain blocks of the region, but there are also both low-angle and high-angle normal faults that occur within the mountain blocks and beneath valleys. The origin of the low-angle normal fault surfaces remains controversial, with some geologists arguing that low-angle normal faults formed in their present orientation, or possibly by reactivation of thrust fault surfaces, while others cite evidence for subsequent rotation of high-angle normal faults to gentle dip by isostatic flexure during unloading of the footwall, and/or rotation of originally high-angle faults in a "collapsing domino" style of deformation. Regardless of the process, the structural geology of southwestern Utah contains both low-angle thrust and normal faults of large areal extent, many of which are cut and offset by younger high-angle normal faults.

The presence of low-angle faults within geothermal reservoir

rocks of Paleozoic age is suspected at the Cove Fort–Sulphurdale KGRA (Huttrer, 1994; Ross and Moore, 1994; J. Moore, personal communication, 2010), at Thermo Hot Springs KGRA (figure 1; J. Moore, personal communications, 2010), and is likely at Fumarole Butte–Abraham Hot Springs KGRA based on geophysical data and regional structural setting (e.g. figure 6 of Mabey and Budding, 1994). Low-angle normal faults also occur within the Roosevelt Hot Springs KGRA (Bruhn and others, 1982), and may reflect footwall deformation caused by flexural uplift and back-rotation in the footwall of the extensive Cave Canyon detachment fault that is exposed in the southern part of the Mineral Mountains (Coleman and others, 1997; Anders and others, 2001). Both outcrop and subsurface data (Smith and Bruhn, 1984; Nielson and others, 1986) suggest that the Cave Canyon fault system projects southwestward towards the Thermo Hot Springs KGRA. On the other hand, Paleozoic rocks are clearly thrust over Mesozoic strata along the Blue Mountain fault to the west of the KGRA, which suggests that carbonate and sandstone strata within the KGRA may be duplicated by relict thrust faults as inferred by Nash and Jones (2010).

An evaluation of low-angle faulting within the Thermo Hot Springs KGRA is the primary focus of this research project. Surface manifestation of the KGRA is a series of hot spring mounds formed by siliceous sinter and eolian sand and silt located along NNE-trending faults in the Escalante Desert floor (figure 2; Mabey and Budding, 1987, 1994). The KGRA is located in the complex volcanic terrain of the Blue Ribbon plutonic lineament, an E-W trending belt of extensive mid-Tertiary volcanism and faulting that was subsequently disrupted by younger normal faulting and eruption of basaltic lavas (Rowley and others, 1978). Gravity and magnetic data suggest that the KGRA is bounded by both N-S and E-W trending normal faults that dip steeply and presumably offset earlier structures related to thrust faulting and/or mid-Tertiary extension (Sawyer, 1977). Drill-hole data from a Republic Geothermal well located southwest of the Hot Spring Mounds penetrated 1148 ft of alluvium, followed by 2000 ft of volcanic rocks, 1772 ft of sedimentary and metamorphic rocks, and bottomed in granite at 7283 ft with a maximum temperature of 345° F at 6562 ft (Mabey and Budding, 1994). This stratigraphy is similar to that found in Raser Technologies wells surrounding their Hatch geothermal plant, where a thrust fault is interpreted to duplicate the carbonate-sandstone section of the reservoir (Nash and Jones, 2010). Metamorphic rocks are sandwiched between the base of the sedimentary section and underlying granite. The sedimentary rocks are presumably Paleozoic or early Mesozoic age based on a comparison of well chip samples with stratigraphic descriptions from outcrops in the surrounding mountains. The metamorphic rocks, some of which are marked “skarn” may be contact metamorphic products of the underlying intrusion (Nash and Jones, 2010), but a similar stratigraphy and deformed metamorphic sequence is present along the Cave Canyon detachment fault at the southern end of the Mineral Mountains (Nielson and others, 1986; Coleman and others, 1997).

The thickness of the Three Creeks Tuff Member of the Bullion Canyon Volcanics in boreholes at the KGRA is much greater than in adjacent areas (J. Moore and J. Bartley, personal communication, 2010). The unusually thick volcanic section is interpreted without benefit of down-hole dip meter data, and tectonic rotation to high dip angle during normal faulting may explain the unusual thickness.

## STRATIGRAPHY AND STRUCTURE OF RASERTECH WELL 17-34

### Overview of Subsurface Work

RaserTech Well 17-34 (figure 2) was chosen for detailed study because a formation XRMI-scanner log is available for analysis of rock structure in the lower part of the borehole. This log provided structural measurements where the borehole penetrated the sequence passing from sedimentary strata into subjacent metamorphic and granitic rock (Nash and Jones, 2010). This geologic section is very similar to that associated with the Cave Canyon detachment fault in the southern Mineral Mountains (Nielson and others, 1986). Although some other wells in the Thermo Hot Springs KGRA penetrate metamorphic and granitic rocks at depth, none of them have a formation XRMI-scanner log.

The following work was completed on samples and logs from well 17-34: (1) visual inspection, petrographic analysis and mineral spectra analysis of chip samples mounted on boards, (2) inspection of petrographic thin sections of wellbore chip samples for fragments of fossils to constrain the age of the limestone units encountered in the borehole, and (3) structural analysis of fractures, faults and compositional layering in the lower part of the borehole where the XRMI-scanner log was collected.

Depths cited in borehole 17-34 are measured along the length of the borehole with the Kelly bushing as datum. The borehole is vertical to a measured depth of about 2200 ft, below which the hole deviates on average 17.7° from vertical to the Total Depth (T.D.) at 9300 ft. The vertical depth at T.D. when corrected for borehole deviation from vertical is roughly 8700 ft.

### Stratigraphy

The stratigraphic section in figure 3 presents our interpretation of the rock units penetrated in well 17-34 based on the petrography, composition, and fossil fragment content of the chip samples obtained during drilling. This stratigraphy is similar to that reported by Nash and Jones (2010) from several wells in the KGRA including well 17-34, but there are significant differences in the assignment of units to various formations, and in the interpretation of the structural geology. The most important conclusions of our study of the stratigraphy are listed below:



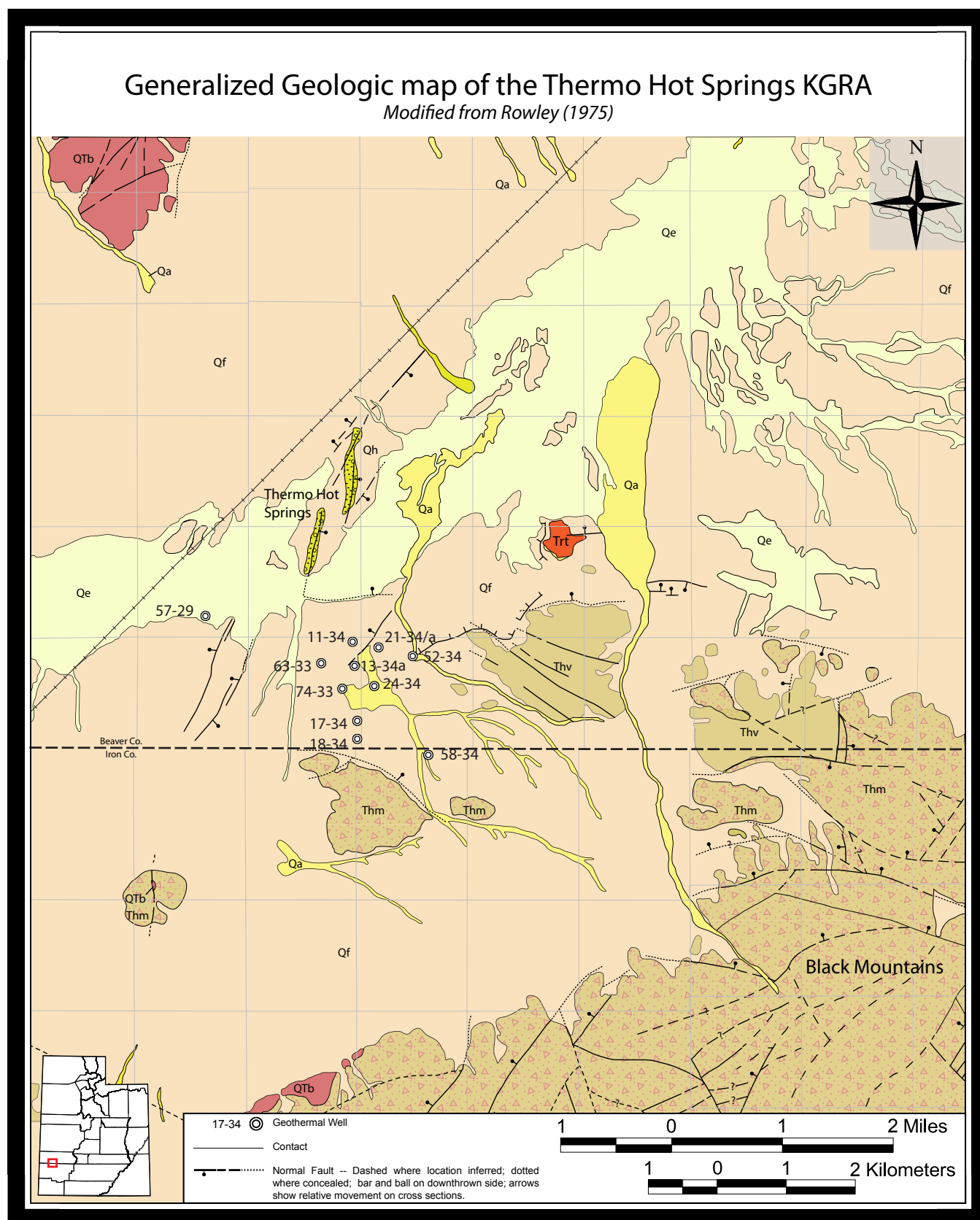


**Figure 2A.** Geological map of the Thermo Hot Springs KGRA with locations of geothermal wells. The map units are described in the map legend (figure 2B).

## Geologic Units of the Thermo Hot Springs KGRA

*Modified from Rowley (1975)*

<p><b>Qa</b> ALLUVIUM (HOLOCENE AND PLEISTOCENE)-Sand and less abundant pebble gravel deposited in intermittent stream channels, on bordering flood plains, and in fans of major drainages. Contact transitional with deposits of Escalante Arm of Lake Bonneville (Qe) in some places. As much as 10 m thick.</p>	<p><b>QTz</b> BASALT LAVA FLOWS (PLEISTOCENE?, PLEISTOCENE, AND MIOCENE)-Resistant black to medium-gray, commonly vesicular or amygdaloidal lava flows of basalt. Basalt generally contains spots of antigorite(?), an alteration product of olivine. This unit also includes scoria and a 3 m thick white tuff that underlies basalt in sec. 16 and 20, T. 31 S., R. 12 W. Some flows overlie and resemble rocks of the mafic member of the Horse Valley Formation (Thm); in these places, age and genesis of parts of the two mapped units may be closely similar. As much as 15 m thick.</p>
<p><b>Qf</b> FAN AND PEDIMENT DEPOSITS (HOLOCENE AND PLEISTOCENE)-Silt, sand, and minor pebble gravel from local sources deposited in alluvial fans and on pediments. Includes minor colluvium. Locally more than 30 m thick. Contacts approximately located.</p>	<p><b>Tt</b> RHYOLITE OF THERMO HOT SPRINGS AREA (MIOCENE)-Light-gray or black resistant flow-foliated, locally spherulitic crystal-poor dome and (or) lava flows of alkalic rhyolite that contain sanidine, quartz, and plagioclase, and traces of biotite, opaque minerals, and hornblende. Mostly devitrified except for a 2 m thick obsidian layer in the southwestern part of the exposure. Has a K-Ar age of 10.3 m.y., and is part of an east-trending alignment of small plugs, domes, and lava flows of alkalic rhyolite (Rowley and others, 1978)</p>
<p><b>Qh</b> HOT SPRING DEPOSITS OF THE THERMO AREA (HOLOCENE AND PLEISTOCENE)-Hot spring deposits of two echelon mounds nearly 10 m high (sec. 21 and 28, T. 30 S., R. 12 W.) that overlie north-striking fractures, probably faults (Petersen, 1973). The main rock type is resistant bulbous and cavernous growths of tan and pale-green bedded opal (siliceous sinter), containing clasts of windblown quartz sand and silt. Travertine also has been reported (Mundorff, 1970), and eolian sand occurs on the tops and flanks of the mounds. About 20 small hot springs, containing water with recorded surface temperatures as high as 90°C, and with an estimated average reservoir subsurface temperature of 200°C (Howell, 1975; Renner and others, 1976), issue from the tops and eastern sides of the mounds along the main controlling faults. The water is high in hydrogen sulfide and dissolved silica (Lee, 1908). The avenues of escape for the water, and perhaps the water reservoir itself, appear to have formed from the intersection, at about 90° from each other, of north- and northeast-striking faults with nearly east-striking faults; east-striking faults occur east of the springs (Rowley and Lipman, 1975).</p>	<p><b>Thv</b> HORSE VALLEY FORMATION (MIOCENE) - Gray or pink, or less commonly white, red, tan, black, purple, brown, soft to resistant, rhyodacite to dacitic lava flows, volcanic mudflow breccia, plugs, and minor ash-flow tuff. Erupted from numerous clustered central vents, most of which are in the quadrangle. Unit is generally poorly exposed, especially where composed of volcanic mudflow breccia, which weathers to boulder-strewn slopes. Where well exposed, volcanic mudflow breccia consists of angular pebble- to bolder-sized clasts of Horse Valley Formation lithology contained in a mostly light-gray or tan muddy matrix, and unsupported by direct contact with each other. Lava flows and plugs are generally flow-foliated. Most of the unit represents vent facies rock, using the terminology of Parsons (1965, 1969) and Smedes and Prostka (1973).</p>
<p><b>Qe</b> DEPOSITS OF ESCALANTE ARM OF LAKE BONNEVILLE (Pleistocene)-Includes clay, silt, sand, and pebble gravel deposited in, and on shorelines of, a Pleistocene lake (Escalante arm of Lake Bonneville). Includes fluvial deposits from streams that emptied into the lake. Much of the unit, however, consists of fluvial deposits formed during terminal drying up of the lake and draining of its water northward to lower parts of the Lake Bonneville topographic basin. Thus most contacts may represent a north-draining channel. Only the most prominent contact is shown; generally, it represents the youngest and lowest shoreline or outlet channel, and has an elevation of 1,530-1,540 m, sloping northward. Locally includes Holocene alluvium. Contact with alluvium (Qa) and fan and pediment deposits (Qf) locally transitional (Lee, 1908).</p>	<p><b>Thm</b> Mafic member of the Horse Valley Formation - Soft to resistant mostly black dacitic to andesitic(?) volcanic mudflow breccia and subordinate lava flows. Volcanic mudflow breccia consists of angular pebble- to boulder-sized clasts contained in a light- to medium-gray, tan, or pink muddy matrix and unsupported by direct contact with each other; breccia weathers to boulder-strewn slopes. Clasts in the breccia and lava flows generally are black, red (devitrified rock), or dark-gray and consist of 15-30 percent plagioclase, 2-11 percent pyroxene, 1-3.5 percent opaque minerals, and, in some specimens, small amounts (generally 1 percent or less) of hornblende set in a glass matrix that contains sparse plagioclase microclots.</p>

**Figure 2B.** Description of geologic units of the Thermo Hot Springs KGRA.

1. The presence of the Carmel Formation below the Tertiary volcanic sequence and above the Navajo Sandstone. Identification of this formation is confirmed by fossil fragments that form a diagnostic Middle Jurassic assemblage based on outcrop studies in Utah by Charette (1998) and De Gilbert and Ekdale (1999).
2. Confirmation that the limestone and sandstone strata between the base of the Lower to Middle Triassic Moenkopi Formation and the top of the metamorphic sequence are upper Paleozoic in age. This age assignment is based upon fossil fragments that include spines from upper Paleozoic brachiopods and abundant crinoid fragments. The fossil assemblage is similar to those described from outcrops of upper Paleozoic rocks elsewhere in Utah (Cheevers and Rawson, 1979; Schubert and Bottjer, 1995). The uppermost limestone unit is the Lower Permian Kaibab Formation. The stratigraphic section then appears to follow a normal sequence with increasing depth that includes the Queantoweap Sandstone (Lower Permian), the Pakoon Dolomite-Callville Limestone (Lower Permian to Pennsylvanian) and the Mississippian Redwall Limestone.
3. We find no compelling evidence for duplication of the sedimentary section by thrust faulting. Our conclusion of a largely intact stratigraphic section is based on (1) comparison of the lithology and mineralogy of the chip samples from the borehole with samples we collected from the Mesozoic and Paleozoic strata exposed in the southern Mineral

Mountains, and (2) no evidence of down-hole repetition of fossil fragment assemblages that would suggest duplication by thrust faulting.

4. We interpret a fault contact at the base of the Redwall Limestone where remnants of contact metamorphic "skarn", and the underlying metamorphic and granite chip samples show evidence of shearing and hydrothermal alteration with the formation of chlorite, sericite, and epidote that is typical of low-angle normal faults exposed in the Mineral Mountains (figure 4; Bruhn and others 1982; 1994), including the large-scale Cave Canyon detachment fault mapped by Nielson and others (1986).

### Structural Interpretation (7660–8770 ft)

The formation XRMI-scanner log acquired in the lower part of well 17-34 provides information on the dip and dip direction of layering in the lower part of the Redwall Limestone, the metamorphic sequence, and underlying granite (figure 5). Figure 5 consists of several parts: (1) a dip-azimuth plot showing the dip direction of compositional and structural layering in the rocks between 7660 and 8623 ft, (2) several lower hemisphere stereographic projection (stereonet) plots showing poles to fractures in the lower, middle and upper parts of the logged interval together with a cumulative fracture pole plot, and (3) a fracture intensity plot as a function of depth, with the number of fractures encountered per 10 ft of logged interval, computed using a running average calculation. Each stereonet uses the Kamb method to contour the expected point density distribution in 2% class intervals in relation to the poles to fracture orientations



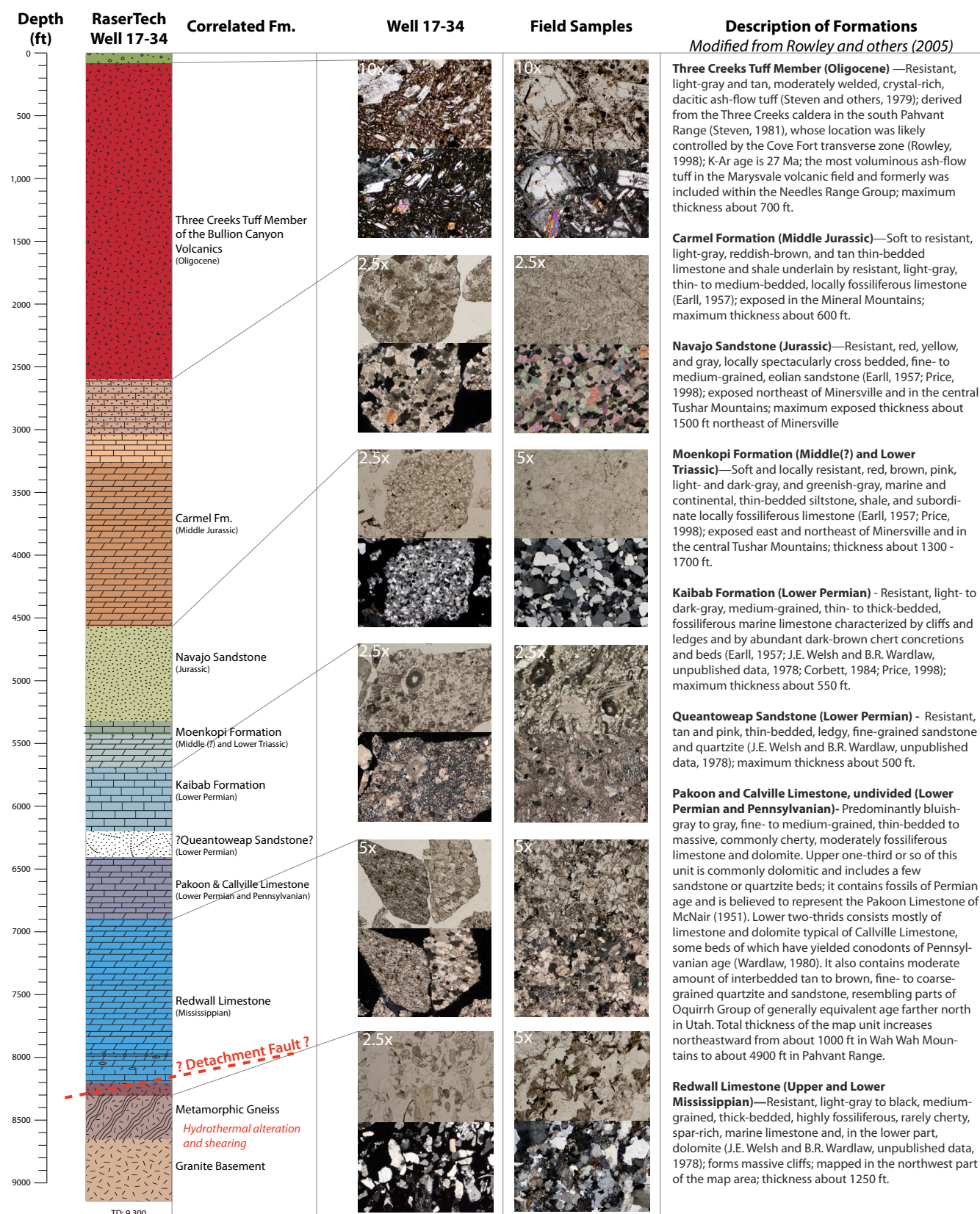


**Figure 3.** Stratigraphic column of well 17-34 based upon comparing rock fragments and mineralogy in thin sections from samples in well 17-34 with thin sections of rocks exposed in the Mineral Mountains, Utah. Rocks exposed in the Mineral Mountains include Tertiary volcanic and sedimentary rock, Mesozoic and Paleozoic strata, together with metamorphic rock, granite and fault-related cataclasite. Images of representative thin sections from the well and equivalent rocks in outcrop are displayed to the right of the stratigraphic column. Much of the rock unit description in the right hand column of text is from Rowley and others (2005) and references cited therein.

(Marshak and Mitra, 1988). The strike and dip of faults are shown (green strike and dip symbols) and summarized in the table at the upper right corner of the figure. Faults are fractures having evidence for offset of layering in the scanner log, and fractures are open cracks. The nature of the layering detected by logging includes, presumably, compositional layering that represents bedding in the lower part of the Redwall Limestone, metamorphic foliation in the gneiss, and perhaps foliated cataclasite and/or moderate dipping joints and faults in the granite.

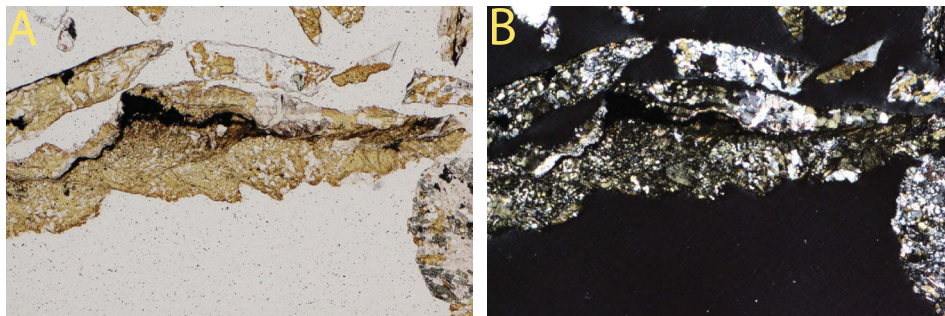
The dip direction of layering is between east and south-south-east proceeding from the base of the logged interval towards the top (figure 5). Dip angles average  $40^{\circ}$  to  $50^{\circ}$  throughout; there is less variation in the angle of dip than in the direction of dip. Proceeding down hole from right to left on the dip-azimuth plot the section between 7660 and 8100 ft is in the lower part of the Redwall Limestone where layering dips to the southeast (light blue line in figure 5). The direction of dip rotates abruptly to the south-southeast in the lowest part of the Redwall Limestone and sheared “skarn” of unit 13 (figure 3), and then rotates counter-clockwise to east-southeast to east in the lower gneiss and granite.

There are only six faults identified in the logged interval (figure 5). The faults dip between  $22^{\circ}$  and  $72^{\circ}$ . Strike directions of five of the faults vary from northeast to northwest, with one striking east-west. The dip-directions are primarily between west and southeast.

Open fractures are much more numerous than the faults, and when considered as a single group they form a conjugate set of moderately to steeply dipping surfaces that strike northward (figure 5, cumulative fracture plot). The bimodal population of fracture poles is present in the upper (light blue dip-azimuth section) and lower (dark blue dip-azimuth section) parts of the logged interval, but in the middle section where the dip azimuth is south-southeast the fracture pole distribution reflects a somewhat different geometry. One set of fractures dips to the west-northwest at moderate to steep angle, and another set dips at low to moderate angle towards the south (figure 5, middle stereonet). The fracture density plot contains several spikes in the frequency of fractures, with several peaks labeled 1–6 and keyed to the dip-azimuth plot. The fracture intensity peaks reach maxima of  $\approx 4.5$  fractures/foot in the lower part of the Redwall Limestone, metamorphic “skarn” and gneiss. The un-

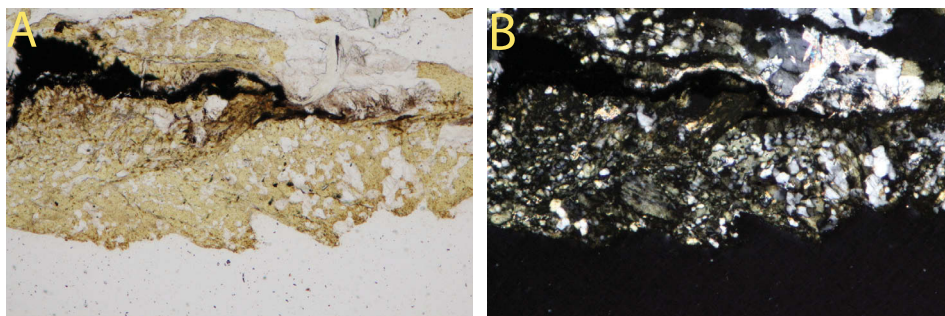
#### Petrographic thin sections of cuttings from well 17-34.

5X



Well 17-34 at 8,100': A) Plane polarized light. B) Crossed nicols. Field of view is 3.12 mm.

10X



Well 17-34 at 8,100': A) Plane polarized light. B) Crossed nicols. Field of view is 1.56 mm.

Variable relief pyroxene altered from calcite. Brown, light green, and white faulted and sheared limestone skarn.

**Figure 4.** Images of a petrographic thin section obtained from the sheared “skarn” deposit in the lower part of well 17-34. The sample shows evidence of shearing and cataclasis that is presumably caused by low-angle or detachment faulting.

labeled peak of 3.3 fractures/foot at 8715 ft is located in the granite. These “raw” fracture intensity values must be corrected to account for the angle of intersection between the well bore and the average poles to the fracture sets when discussing aspects of permeability in the lower part of the reservoir.

The east to southeast dip azimuth of layering logged in the lower part of well 17-34 is apparently representative of the contacts between the Redwall Limestone and underlying metamorphic rocks and granite. Nash and Jones (2010) produced several geological cross sections through the KGRA that include a west to east line between wells 63-33 and 52-34, and a northwest to southeast line between wells 29-57 and 24-24 (See figure 2 for well locations). In both cross sections they show the contact between the lowermost limestone and the metamorphic rocks dipping towards the east to southeast at 25°–30°. This range of dip angle is about 10° less on average than in the XRMI-scanner log, but the cross section angles are averaged over distances up to 2 miles (3.2 km) while the XRMI-scanner log is a point-type structural measurement.

The conjugate open fracture sets are reminiscent of joints and small faults with minimal shearing offset that form in extensional stress regimes. When viewed on the cumulative fracture stereonet in figure 5, the conjugate fracture pattern suggests an extensional stress field with the maximum principal compressive stress ( $s_1$ ) oriented nearly vertical, and the least compressive stress ( $s_3$ ) oriented roughly east-west. This stress field is consistent with the regional direction of extension in the Basin and Range Province, and the orientation of the generally north-trending normal faults that are associated with the Thermo Hot Springs KGRA (figure 2). The tendency for the fractures to be “open” and detectable on the XRMI-scanner log may be related to their orientation in the contemporary stress field, where the moderate to steeply dipping fractures are critically, or nearly critically, oriented for failure by shearing along the rough fracture walls. Distortion of asperities (“bumps”) along fracture walls opens void space and enhances fluid permeability (Brown and Bruhn, 1996). We will return to this topic when discussing the permeability structure of the reservoir based upon the analog outcrops that are exposed in the central and southern Mineral Mountains.

## MINERAL MOUNTAINS ARE AN ANALOG TO THE KGRA RESERVOIR?

### Stratigraphic and Structural Similarities

The stratigraphy and structure of the rocks in well 17-34 are similar to those of rocks exposed in the central and southern Mineral Mountains, which in our opinion provide a useful analog to the Thermo Hot Springs geothermal reservoir. Striking similarities include: (1) Quaternary and Tertiary volcanic and intercalated sedimentary rocks that overlie a sedimentary section that extends from the Carmel Formation down into

the Redwall Limestone, (2) Tertiary granite intruded into Precambrian schist and gneiss, and into upper Paleozoic strata that includes the Redwall Limestone, (3) low-angle normal faulting within the granite and base of the Paleozoic rocks—this includes the large Cave Canyon detachment fault that has at least several kilometers of top-to-west displacement, and is marked by hydrothermally altered cataclasite and breccia, and (4) a mosaic of high-angle normal and oblique-slip faults that include both north- and east-trending fault sets.

### Detachment Faulting

The Cave Canyon detachment fault is the largest of several low-angle normal faults exposed in the Mineral Mountains (Bruhn and others, 1982; Nielson and others, 1986). The fault separates Oligocene to Miocene granitic rocks of the Mineral Mountains intrusive complex from overlying Paleozoic strata. The fault zone contains cataclasite up to 656 ft thick. Hydrothermal alteration of the granitic cataclasite formed chlorite, epidote and sericite, which suggest that faulting occurred at temperatures of 302° to 572° F (Barnett and others, 1996), and during early stages at depths near the transition from quasi-plastic to frictional deformation in the fault zone according to Nielson and others (1986).

The Cave Canyon fault is exposed because of uplift and exhumation of the central Mineral Mountains (Nielson and others, 1986). Intrusive activity overlapped with movement on the detachment fault circa 9 Ma, and was followed by uplift and exhumation of the range. The detachment fault is truncated by the Cherry Creek Fault (figure 6), which dips steeply towards the south and contains a thick section of Tertiary through upper Paleozoic rock in its hanging wall. Detachment faulting was accompanied by the formation of north and east trending faults that dissect the upper plate of the detachment fault, and may merge into or abut against the detachment at depth. Eastward tilting of these strata together with preservation of a mosaic of north and east trending normal and oblique-slip faults (figure 7) suggests that the detachment fault continued south of the Cherry Creek Fault, and lies beneath the southern end of the Mineral Mountains. We propose that this structure may also occur in the Thermo Hot Springs KGRA, where juxtaposition of the Redwall Limestone against altered metamorphic rock and granite is similar to the structural relationship observed where the Cave Canyon detachment fault is exposed in the Mineral Mountains (e.g. Bruhn and others, 1982; Nielson and others, 1986).

### Permeability Structure of Analog Outcrops

The effects of faulting and jointing on permeability were documented at several localities in the Mineral Mountains where rocks equivalent to those in the Thermo Hot Springs KGRA reservoir are exposed in outcrop. Specific examples include localities where upper Paleozoic strata are faulted against granite on low-angle normal (detachment) faults, where there is intense jointing and brecciation of the Queantowep Sandstone, and



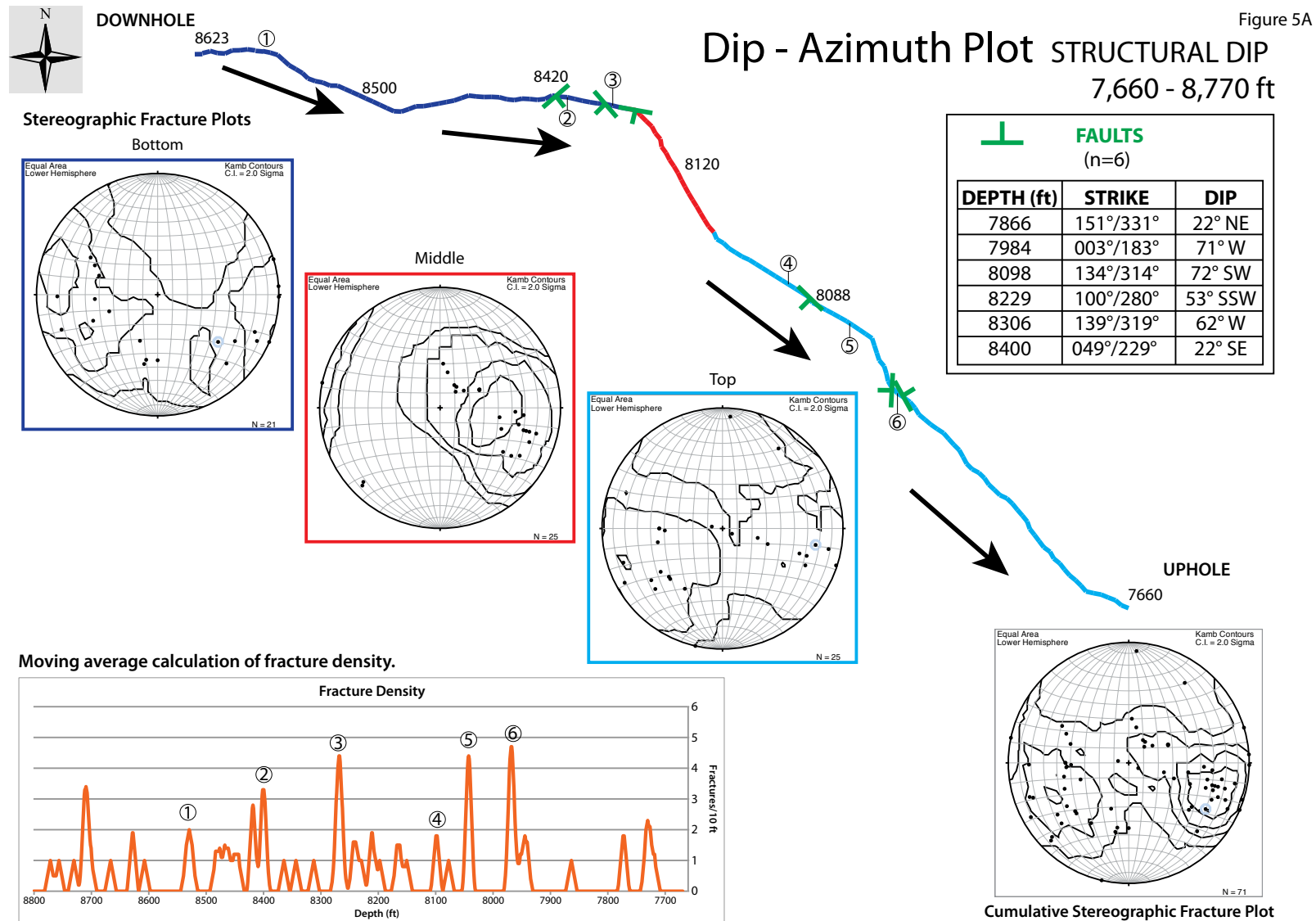


**Figure 5.** The formation XRMI-scanner log data was acquired in the lower part of well 17-34. The structural interpretation of this data consists of several parts: (1) A dip-azimuth plot showing the dip-direction of compositional and structural layering in the rocks from 7660–8623 ft. From left to right across the plot black arrows indicate the averaged dip orientation from bottom to top of the logged interval. There are only six faults identified in the logged interval. They are plotted in green strike and dip symbols along the dip-azimuth plot. The individual orientations of each structure are summarized in a table in the upper right corner. (2) Depth along the dip-azimuth plot is broken into 3 sections from left to right: bottom (dark blue), middle (red), and top light blue. These sections have been color-coded to the corresponding stereographic projection (stereonet) plots showing poles to fractures. The bottom right corner of the figure is a cumulative fracture pole plot of all 71 fractures. The subsurface positions of these stereographic projection plots along well 17-34's directional drill path can be seen in figure 5B. (3) A fracture intensity plot as a function of depth, with the number of fractures encountered per 10 ft of logged interval, computed using a running average calculation. Several spikes in the frequency of fractures, with several peaks labeled 1–6 and correlated to depth along the dip-azimuth plot.



Figure 5B

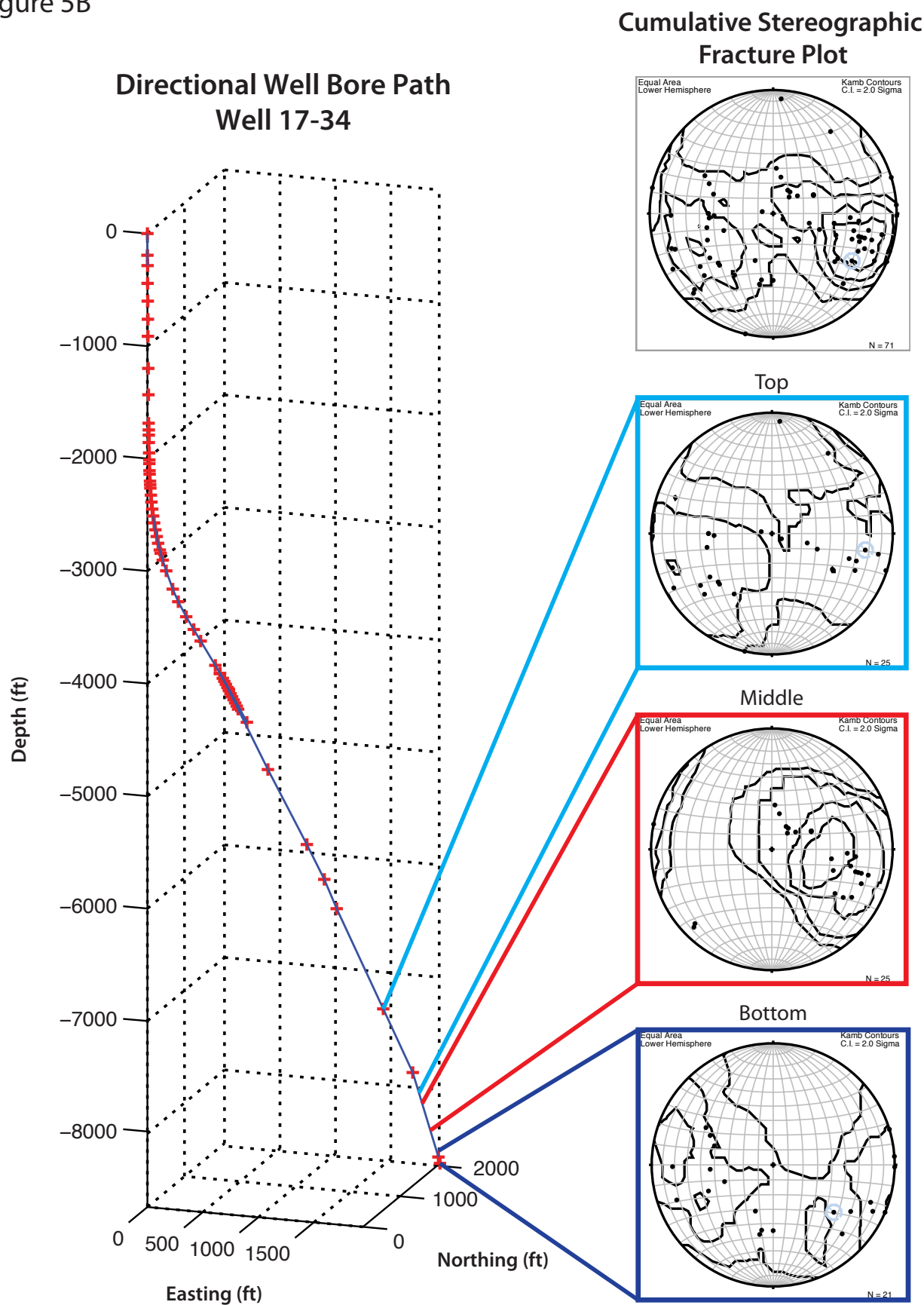
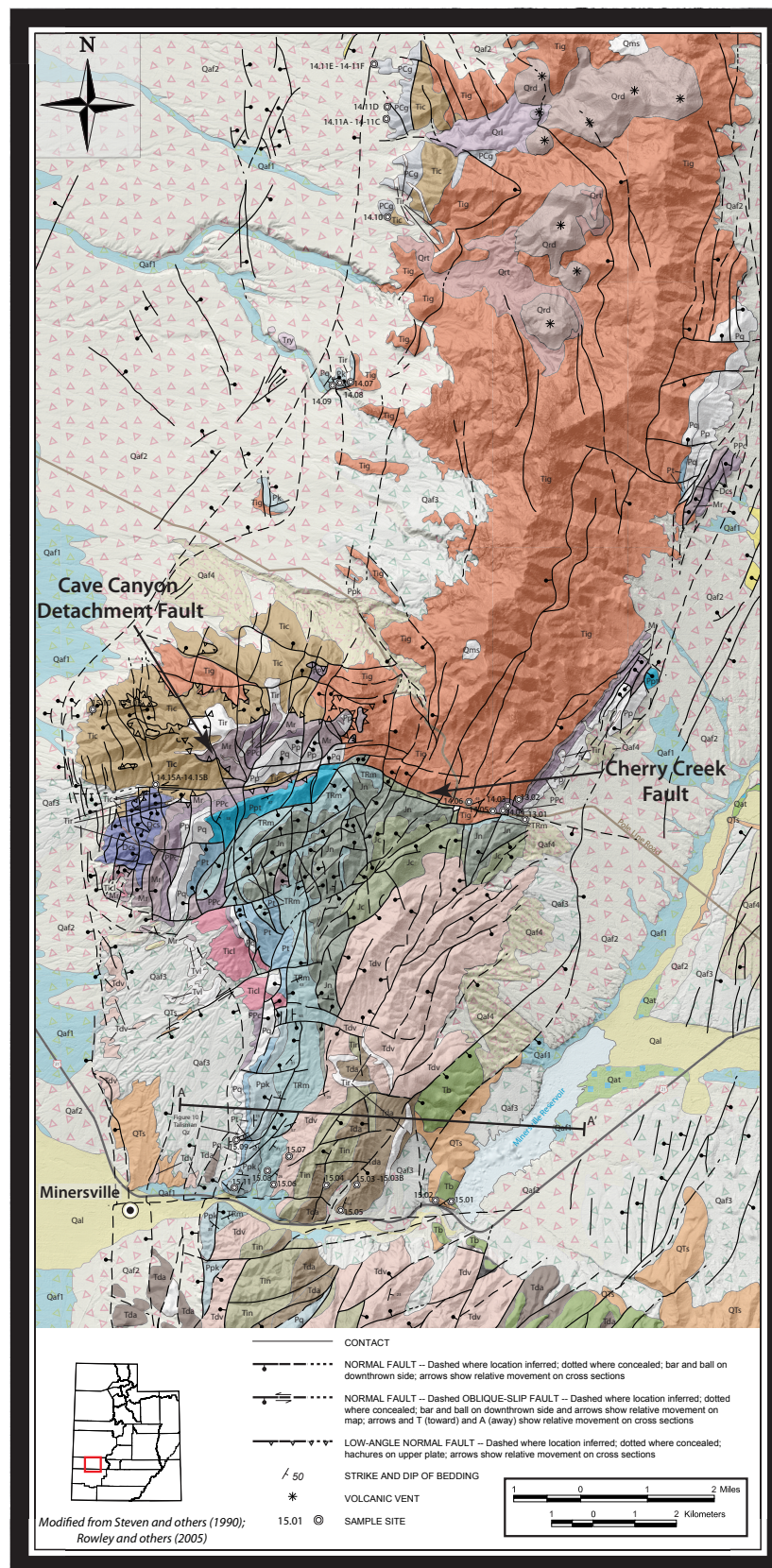


Figure 5. Continued.



**Figure 6A.** Geologic map of the southern Mineral Mountains showing the formations and faults. Note the line of cross section A-A' which is shown on figure 7. Sample sites markers indicate where outcrop samples were taken for petrographic and chip board analysis. See figure 1 for location of the map figure. The map is created by draping part of the 1° x 2° geologic map of Steven and others (1990) and part of the 30' x 60' geologic map of Rowley and others (2005) over 5 m – posted digital elevation model obtained from the Utah GIS Portal. The map explanation, modified from Steven and others (1990) and Rowley and others (2005) is shown in figure 6B.

## Description of Geologic Units of the Southern Mineral Mountains, Beaver County, Utah.

*Modified from Steven and others (1990);  
Rowley and others (2005)*

<b>Qal</b>	Alluvium—Sand, gravel, silt, and clay in channels, floodplains, and adjacent low river terraces of rivers and major streams; maximum thickness about 30 ft.	<b>Tdv</b>	Mount Dutton Formation—Vent facies—Volcanic mudflow breccia, flow breccia, and lava flows interpreted to represent near-source eruptions (Anderson and Rowley, 1975); many of the source stratovolcanoes are aligned east-west along the east-striking Blue Ribbon transverse zone (Rowley and others, 1978, 1998; Rowley, 1998), which passes west from Kingston Canyon along the break in slope between the Tushar Mountains and Markagunt Plateau, then along the north side of the Black Mountains and on across the entire Great Basin.
<b>Qat</b>	Young stream-terrace deposits—Sand and gravel that form dissected surfaces as much as 15 ft above the level of adjacent modern streams; maximum thickness about 10 ft.		
<b>Qaf</b>	Qaf1 - Young alluvial-fan deposits—Poorly to moderately sorted silt, sand, and gravel deposited by streams, sheetwash, debris flows, and flash floods on alluvial fans and on coalesced alluvial fans and pediments (pedmont slopes); surface is modern and generally undissected; thickness at least 30 ft.  Qaf2, Qaf3, Qaf4 - Middle alluvial-fan deposits—Poorly to moderately sorted silt, sand, and gravel deposited by streams, sheetwash, debris flows, and flash floods on alluvial fans and on coalesced alluvial fans and pediments (pedmont slopes); surface is moderately dissected by modern streams; subscript denotes relative age, with Qaf2 youngest and Qaf4 oldest (Machette and others, 1984); thickness at least 50 ft.	<b>Tda</b>	Alluvial facies—Primarily volcanic mudflow breccia in which lithologies are more heterogeneous than in the vent facies, representing deposits interpreted to have traveled farther from the source, down the flank of individual stratovolcanoes (Anderson and Rowley, 1975), passing into conglomerate still farther from the source; the unit is by far the most voluminous component of the formation.
<b>Qms</b>	Landslide deposits—Unsorted, mostly angular, unstratified rock debris moved by gravity from nearby bedrock cliffs; maximum thickness about 100 ft.	<b>Tic</b>	Calc-alkaline intrusive rock—Moderately resistant, gray, tan, pink, and brown, crystal-rich monzonite, low-silica granite, granodiorite, and monzodiorite; the calc-alkaline sources of Tic and several other volcanic units, and the calc-alkaline early products of the Mineral Mountains batholith; plutons of Tic, Tig, and other intrusive units represent cupolas of a large composite batholith that underlies the east-trending Pioche-Marysvalde igneous belt (Rowley, 1998), including the central and north part of the Marysvalde volcanic field, and extends westward beyond the Nevada border, as indicated by geophysics (Steven and Morris, 1987; Rowley, 1998; Campbell and others, 1999; Rowley and others, 2002) and geologic mapping (Steven and others, 1990); isotopic ages of Tic cluster at about 25 to 23 Ma (Steven and others, 1979; Cunningham and others, 1984a; Nielson and others, 1978, 1986; Aleinikoff and others, 1986; Coleman and others, 2001).
<b>Qrd</b>	Rhyolite of Mineral Mountains—High-silica rhyolite made up of three types of deposits erupted from sources in the Mineral Mountains and derived from the vestiges of the same magma chamber that resulted in the Mineral Mountains batholith; rhyolite largely deposited on the eroded surface and canyons cut in that batholith; Volcanic dome—Resistant, mostly tan, crystal-poor (sparsely porphyritic), perlitic-mantled, flowfoliated, high-silica rhyolite lava flows, flow breccia, and minor tuff that form volcanic domes by deposition around central vents; K-Ar age about 0.6 to 0.5 Ma (e.g., Lipman and others, 1978; Sibbett and Nielson, 1980); maximum thickness about 900 ft.	<b>Jc</b>	Carmel Formation—Soft to resistant, light-gray, reddish-brown, and tan thin-bedded limestone and shale underlain by resistant, light-gray, thin- to medium-bedded, locally fossiliferous limestone (Earl, 1957); exposed in the Mineral Mountains; maximum thickness about 600 ft.
<b>Qrt</b>	Tuff—Poorly consolidated, white, unwelded, pumice-rich, crystal-poor, high-silica rhyolite ashflow and airfall tuff; best exposed in Ranch Canyon, where mined for pumice; overlain by Qrd (Nash and Smith, 1977; Machette and others, 1984; Machette, 1985); K-Ar age about 0.8 to 0.6 Ma (Lipman and others, 1978); exposed thickness as much as 600 ft.	<b>Jn</b>	Navajo Sandstone—Resistant, red, yellow, and gray, locally spectacularly cross bedded, fine- to medium-grained, eolian sandstone (Earl, 1957; Price, 1998); exposed northeast of Minersville and in the central Tushar Mountains; maximum exposed thickness about 1500 ft.
<b>QTs</b>	Sevier River Formation—Poorly to moderately consolidated, tan and gray, tuffaceous sandstone and subordinate mudstone, siltstone, and conglomerate deposited in basins of different ages (Pliocene to late Miocene) and origins; basins were formed by normal faults and subordinate oblique and strike-slip faults related to the youngest basin-range extension that is responsible for the present topography (Rowley and Dixon, 2001; Rowley and others, 2002); deposits generally consist of fanglomerate near the present basin margins, piedmont slope deposits farther toward the centers of the basins, and lacustrine deposits near the centers of the basins; thickness of QTs at least 2000 ft.	<b>TRm</b>	Moenkopi Formation—Soft and locally resistant, red, brown, pink, light- and dark-gray, and greenish-gray, marine and continental, thin-bedded siltstone, shale, and subordinate locally fossiliferous limestone (Earl, 1957; Price, 1998); exposed east and northeast of Minersville and in the central Tushar Mountains; thickness about 1300 to 1700 ft.
<b>Tb</b>	Basalt lava flows—Resistant, dark-gray and black, locally vesicular or amygdaloidal, crystal-poor (olivine and pyroxene phenocrysts) olivine basalt lava flows, flow breccia, and cinder cones; synchronous with basin-range extension (Christiansen and Lipman, 1972; Rowley and Dixon, 2001); includes basalt southeast of Otter Creek Reservoir that has a K-Ar date of 5.0 Ma (Best and others, 1980), that has a K-Ar date of 7.6 Ma, (Rowley and others, 1981); maximum thickness of lava flows about 200 ft.	<b>Ppt</b>	Plympton, Kaibab, and Toroweap Formations, undivided
<b>Try</b>	Young rhyolite lava flows—Small, resistant, mostly gray, flow-banded, crystal-poor, high-silica rhyolite volcanic domes and subordinate pyroclastic material, most of which help define an east-trending structural belt known as the Blue Ribbon transverse zone (Rowley and others, 1978; Rowley, 1998); also includes a small dome in Corral Canyon, west of the Mineral Mountains, that has a K-Ar date of 7.9 Ma (Lipman and others, 1978; see also Evans and Steven, 1982); in most other places the maximum thickness of the rhyolites is less than 200 ft.	<b>Pk</b>	Kaibab and Toroweap Formations, undivided—Mapped only in the central Tushar Mountains, where their combined thickness is 500 to 800 ft.
<b>Tir</b>	Rhyolite porphyry—Resistant, mostly small, gray, tan, and pink, commonly hydrothermally altered dikes, sills, plugs, a laccolith(?), and masses of other shapes of mostly crystal-poor (phenocrysts of K-feldspar, quartz, plagioclase, and biotite); mostly high-silica rhyolite and fine-grained (Sibbett and Nielson, 1980) that intrudes rocks as young as the main granitic batholith of the Mineral Mountains (Tig) and has K-Ar dates of 9.1 and 9.6 Ma (Nielson and others, 1986), a U-Pb zircon date of 11.0 Ma (Coleman and Walker, 1994), and an Ar/Ar date of 11.5 Ma (Coleman and others, 2001); low-silica, altered, crystal-poor (phenocrysts of plagioclase and minor sanidine, biotite, and hornblende) rhyolite dikes and plugs in the south Mineral Mountains that have K-Ar dates of 22.5 and 22.3 Ma (Rowley and others, 1994) and may be associated with the calc-alkaline Lincoln Stock (Ticd); as much as several hundred feet across and more than a mile long.	<b>Pt</b>	Toroweap Formation—Generally resistant, light- to dark-gray, black, and tan, fine-grained, mostly thin-bedded, ledgy, locally cherty and fossiliferous, marine limestone and subordinate sandstone (J.E. Welsh and B.R. Wardlaw, unpublished data, 1978; Corbett, 1984); mapped in the northwest part of the map area, where the maximum thickness is about 300 ft.
<b>Tig</b>	Granitic intrusive rocks—Mostly resistant, mostly gray, high-alkali and mostly high-silica (bimodal igneous episode that is synchronous with basin-range extension) granite and related rocks; to the west, in the Mineral Mountains, includes the main mass of the Mineral Mountains batholith, the largest exposed batholith in Utah, which is made up of individual stocks and sheeted dike-like masses of fine- to coarse-grained or porphyritic, nonfoliated, mostly granite (classification of intrusive rocks from International Union of Geological Sciences) but locally monzonite and syenite (Sibbett and Nielson, 1980; Nielson and others, 1978, 1986; Coleman, 1991; Meschter McDowell and others, 2004) Coleman and others (2001) interpreted on the basis of U-Pb zircon and 40Ar/39Ar dates that the main granitic batholith in the Mineral 40 39 Mountains has an age of about 18 to 17 Ma.	<b>PIPqc</b>	Talisman Quartzite (Lower Permian), Pakoon Dolomite, and Callville Limestone, undivided—Mapped only in the central Tushar Mountains, where their combined thickness is about 300 ft although the base is not exposed.
		<b>Pq</b>	Queantoweap Sandstone—Resistant, tan and pink, thin-bedded, ledgy, fine-grained sandstone and quartzite (J.E. Welsh and B.R. Wardlaw, unpublished data, 1978); mapped in the northwest part of the map area; maximum thickness about 500 ft.
<b>Tvl</b>	Local volcanic rocks of the Lincoln Stock—Soft, mostly reddish-brown, hydrothermally altered, dacitic to andesitic lava flows and volcanic mudflow breccia located just west of, and adjacent to, Ticd; about 300 ft thick, but its base is not exposed; possibly vented products of the Lincoln Stock.	<b>Pp</b>	Pakoon Dolomite—Alternating soft and resistant, light- to dark-gray and pink, ledgy and cliffy, medium-grained, thick-bedded, locally chert-bearing, marine dolomite and subordinate to minor sandstone (J.E. Welsh and B.R. Wardlaw, unpublished data, 1978; Corbett, 1984; Price, 1998); mapped in the northwest part of the map area; thickness about 800 ft.
<b>Tid</b>	Lincoln Stock—Resistant, light-gray, monzonite and granodiorite porphyry stock in the south Mineral Mountains (Earl, 1957; Corbett, 1984; Price, 1998), resulting in contact metamorphic lead-zinc-gold ore deposits of the Lincoln and Bradshaw mining districts; interpreted here to represent a calc-alkaline phase of the Mineral Mountains batholith; has a K-Ar date of 21.9 Ma (Bowers, 1978) and a preliminary U-Pb zircon date of about 23 Ma (Coleman and others, 1997,	<b>Mr</b>	Redwall Limestone—Resistant, light-gray to black, medium-grained, thick-bedded, highly fossiliferous, rarely cherty, spar-rich, marine limestone and, in the lower part, dolomite (J.E. Welsh and B.R. Wardlaw, unpublished data, 1978); forms massive cliffs; mapped in the northwest part of the map area; thickness about 1250 ft.
		<b>Dcs</b>	Crystal Pass Formation, Simonson Dolomite, and Sevy Dolomite, undivided—Mapped only in the northwest part of the map area along the west fault scarp of the south Mineral Mountains. Crystal Pass Formation—Mostly soft, light-gray, thin- to medium-bedded, interbedded marine dolomite and sandstone (J.E. Welsh and B.R. Wardlaw, unpublished data, 1978); thickness about 160 ft. Simonson Dolomite—Resistant, light- to medium-gray, mostly thick-bedded, marine dolomite (J.E. Welsh and B.R. Wardlaw, unpublished data, 1978); thickness at least 500 ft but no complete section is exposed. Sevy Dolomite—Mostly resistant, light-gray siltstone and cross-bedded sandstone at the top, underlain by light-gray marine dolomite; thickness less than 100 ft but only the top of a complexly faulted section in the Bradshaw mining district is exposed.
		<b>pCg</b>	Banded gneiss—Resistant, light- to dark-gray biotite, quartz, K-feldspar, hornblende, and plagioclase gneiss and local schist exposed along the west frontal fault of the Mineral Mountains; as mapped, unit includes local dikes and apophyses of Tertiary intrusive rocks of the Mineral Mountains batholith (Nielson and others, 1986); Rb-Sr and U-Pb dating shows that the unit was last metamorphosed at about 1750 Ma (Aleinikoff and others, 1986).

**Figure 6B.** Description of geologic units of the southern Mineral Mountains.



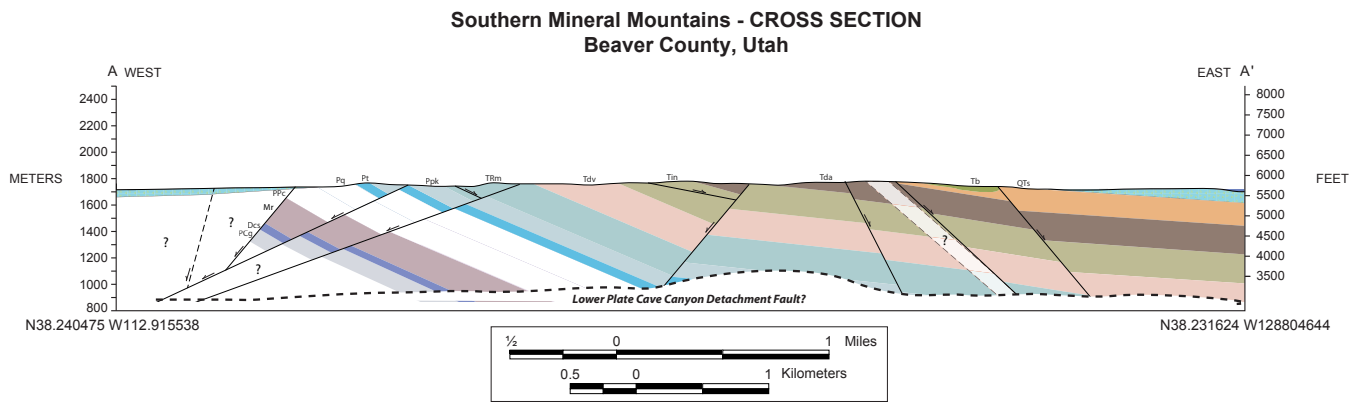


**Figure 7.** Geological cross section along line A-A' on the geological map in figure 6. The rocks are cut by numerous normal faults, most of which dip to the west.

where east-trending normal faults cut the Kaibab Limestone. Each locality provides field evidence concerning structural controls on fluid permeability that may be of use when evaluating the reservoir and fluid migration pathways at Thermo Hot Springs KGRA. The results presented here are preliminary discussions of work that is to be completed as part of W. Anderson's M.S. thesis at the University of Utah.

### Locality 1: Low-angle normal fault near Corral Canyon

The low-angle normal fault near Corral Canyon on the western flank of the Mineral Mountains provides insight into the structure and mineralogy of part of the detachment fault system (figure 8; Bruhn and others, 1982, 1994). The fault dips gently to the west and contains a complex assemblage of variably altered granite cataclasite (figure 8A). Upper Paleozoic limestone and

quartzite in the hanging wall are in fault contact and brecciated along the upper part of the fault zone (Bruhn and others, 1982, 1994; Barnett and others, 1996). The granite beneath the cataclasite zone is intensely fractured with linear intensities of 4–5 fractures/foot, similar to the fracture density recorded in well 17-34 (figure 5) when corrected for the direction of the borehole with respect to the fracture surfaces. The fractures strike approximately normal to the slip direction on the low-angle fault zone, and dip steeply into the granite. Where exposed in the wall of stream cuts the fractures are up to several tens of feet long (figure 8B).

The cataclasite within the fault is comminuted and hydrothermally altered granite with abundant hydrothermal chlorite, epidote, sericite and hematite (Bruhn and others, 1994; Barnett and others, 1996). Stable isotope and geochemical analyses of the cataclasite indicate that alteration occurred during a rela-

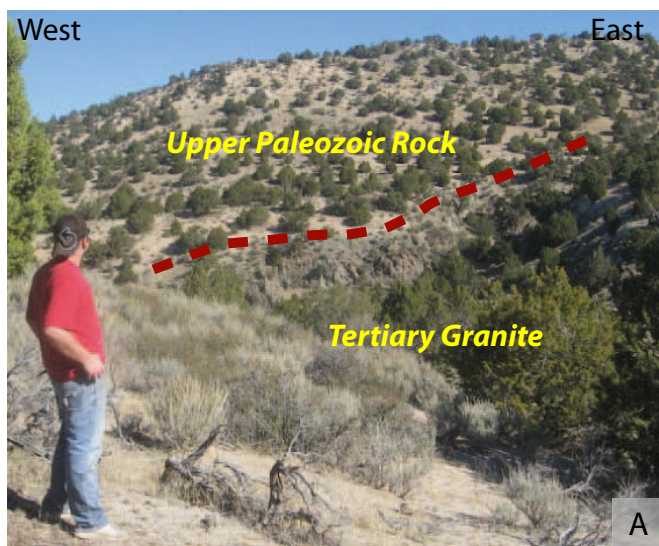
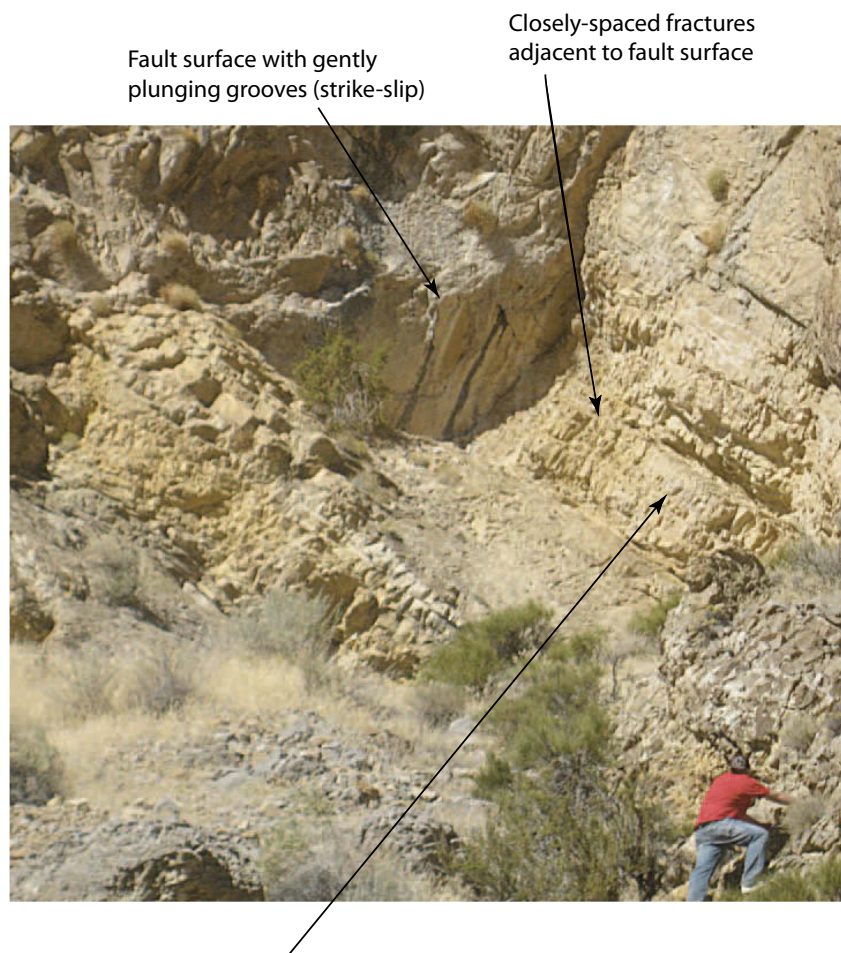


**Figure 8.** Photographs showing the low-angle detachment fault near Corral Canyon on the western flank of the Mineral Mountains. A. View of the fault with granite in the footwall and Paleozoic strata in the hanging wall. B. View of the closely spaced fractures formed in the granite just below the detachment fault. Location is approximately 38.392 N, -112.872 W.



### FAULTED KAIBAB FORMATION AS ANALOG RESERVOIR STRUCTURE



Note that fracture spacing increases away from the fault surface. Also, bedding becomes visible dipping to right as fracture spacing decreases. Fault surface may be relatively impermeable because of comminution of rock into small fragments and secondary cementation. Fluid permeability adjacent to the fault surface may be large if closely spaced joints are oriented for extension or shearing in the ambient stress field.

**Figure 9.** Fracturing and faulting of the Kaibab Formation that illustrates how high-angle faulting affects the rock. The fault is a grooved surface surrounded by a thin layer of cataclasite. Intense fracturing is developed in the adjacent hanging and footwalls. Location is 38.246 N, -112.893 W.

tively short time span, and presumably sealed the cataclasite by mineral alteration and precipitation. The implication is that because of comminution of mineral grains the low-angle fault zone sealed rapidly and became a barrier rather than conduit to fluid flow once faulting ceased. This is a typical process in fault zones, and suggests that low-angle faults may become barriers to upward migration of fluids unless breached by younger and more steeply dipping faults. On the other hand, intense fracturing of granite beneath the cataclasite will create substantial fracture permeability and pathways for lateral migration of fluid over large areas beneath detachment faults.

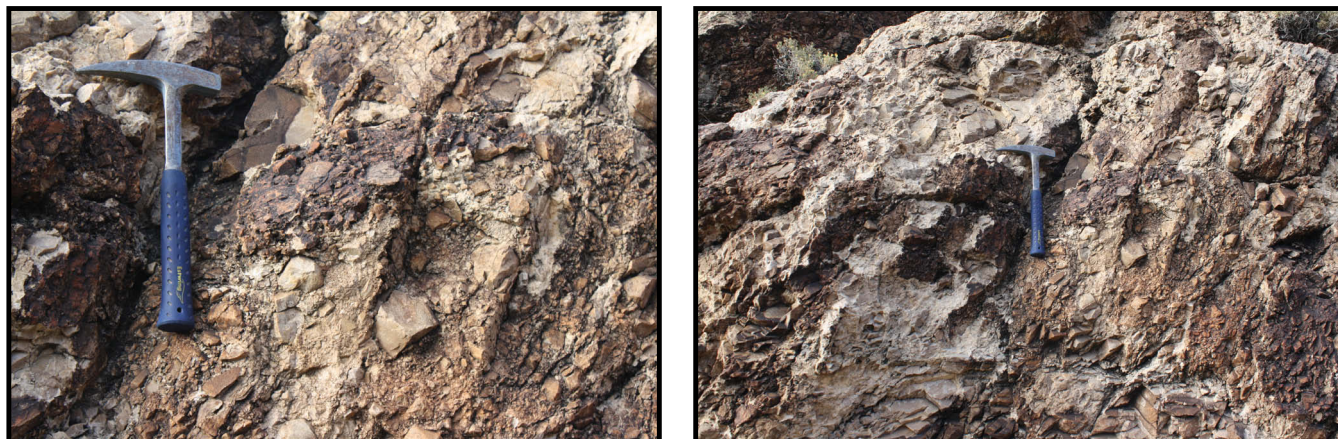
#### Locality 2: Faulting of Kaibab Formation and Queantoweap Sandstone

A mesh-like mosaic of high-angle faults cuts the volcanic and

sedimentary rocks in the southern Mineral Mountains (figure 6). We studied faults and jointing in cliffs composed of Kaibab Formation and Queantoweap Sandstone at a canyon on the western side of the range. Several faults are exposed in the walls of the canyon, and these exposures provide ample evidence of the fault-related structures in limestone and quartzite. The largest faults strike roughly east-west and dip steeply in the canyon. Grooves on some east-striking fault surfaces plunge at low to moderate angles indicating a significant component of strike-slip movement.

Faulting in the Kaibab Formation is marked by discrete slip surfaces that are enveloped by thin layers of cataclasite and surrounded by intensely jointed wall rock (figure 9). The joint intensity decreases rapidly away from the fault surfaces and in general the original sedimentary layering is preserved. Small

## Queantoweap Sandstone (Lower Permian)



Photos taken during fieldwork in the southern Mineral Mountains, Beaver County, Utah.  
November 11, 2011

**Figure 10.** Brecciated Queantoweap Sandstone at the same locality as that shown in figure 9. The brittle quartzite is much more fractured than the adjacent limestone. Location is 38.246 N, -112.893 W.

solution cavities are relict features of paleo-karst that may enhance the permeability of the formation at depth in a geothermal system.

The Queantoweap Sandstone crops out near the base of the cliffs and along the canyon floor. The fracture frequency is much higher in the quartzite than in the adjacent limestone because of its brittleness, or low fracture toughness compared to limestone. In some outcrops the quartzite is brecciated to the point that the original bedding is no longer discernable (figure 10).

### RAPID SPECTRAL DISCRIMINATION OF LITHOLOGY

#### Spectral Analysis of Chip Sample Boards

Mineral spectra were collected from both well 17-34 and outcrop chip samples for a preliminary experiment to determine the efficacy of using a portable spectrometer to rapidly discriminate between rock types using mineral assemblage spectra. The motivation is that petrographic and x-ray analysis of chip samples is both tedious and time consuming. The results show some promise but computer processing will need to be refined before the procedure can be considered robust and useful.

#### Spectral Analysis

Outcrop chip samples, created by crushing rocks collected from the Mineral Mountains, were glued to boards to mimic the

mounting and presentation of drilling chip samples obtained from well 17-34 at Thermo Hot Springs (figure 11). The Mineral Mountains chip samples were treated as standards because they are a known rock type from a formal geological map unit. The chip samples from well 17-34 are considered unknowns to be matched as best as possible with the standards by discrimination of mineral assemblage spectra for wavelengths between visible (V), near infrared (NIR), and short wavelength infrared (SWIR).

Mineral spectra were collected using an ASD FieldPro 2 spectrometer manufactured by Applied Spectral Devices, Inc. of Boulder, CO. The spectrometer records the intensity of reflected light at 10 nm intervals between 350 and 2500 nm. Each spectrum is therefore an ensemble of 2151 measurements of reflected light intensity. Stated in another manner, each measurement is a vector in  $n = 2151$  dimensional space with units of reflectance. Given an unknown material described by vector  $\langle A \rangle$  and a standard or known material described by spectral vector  $\langle B \rangle$  a measure of similarity is the angle ( $\alpha$ ) between the two vectors in  $n$ -space. This angle is given by the expression:

$$\alpha = \cos^{-1} \left( \frac{\sum_{n=1}^{2151} A_n * B_n}{(|\langle A \rangle| * |\langle B \rangle|)} \right)$$

The summation is over the vector components ( $n$ ). The algorithm is referred to as "Spectral Angle Mapper" (SAM) (Kruse and others, 1993). If the angle  $\alpha$  between two materials is smaller than a defined threshold, then the materials are considered matched. We obtained five measurements of each standard sample, found the average vector and then computed the spread in angles ( $\delta\alpha$ ) between each sample in the standard ensemble



and the average vector. The maximum  $\delta\alpha$  was then defined as the threshold value for that standard sample.

The SAM algorithm was implemented in a MatLab computer script with graphical output (figure 12). For each unknown chip sample from well 17-34 we averaged three spectral measurements, and then used the average vector in an attempt to match the unknown with a standard from the Mineral Mountains outcrop samples. The angle  $\delta\alpha$  is plotted against depth of samples in well 17-34, with the interval for the interpreted unit at that depth indicated by a colored rectangle. The width of the rectangle indicates the  $\delta\alpha$  range required for a “match”. Note that if one knew nothing about the stratigraphy in the well there would be difficulty in assigning a unit to a specific depth interval. On the other hand, there are some matches that suggest further refinement of the technique is warranted (for example, basalts near the top of the well bore, the Three Creeks Tuff Member of the Bullion Canyon Volcanics, the Moenkopi Formation, and

the cataclasite and the gneiss). Future work could include (1) collection of spectra in outcrop to make a much more complete library of standard spectra from outcrop strata instead of using only a few samples from a map unit and (2) substitution of other discrimination algorithms, including neural networks. At this point we simply conclude that the spectral matching technique holds promise for rapid classification of well chip samples if a reliable library of standards is created using representative samples of rock units exposed in outcrop.

## IMPLICATIONS FOR GEOTHERMAL RESOURCES

The close correspondence between the geology of the southern Mineral Mountains and that encountered in the Thermo Hot Springs KGRA serves to reinforce the hypothesis that large volumes of hot fluids may lie beneath low-angle faults

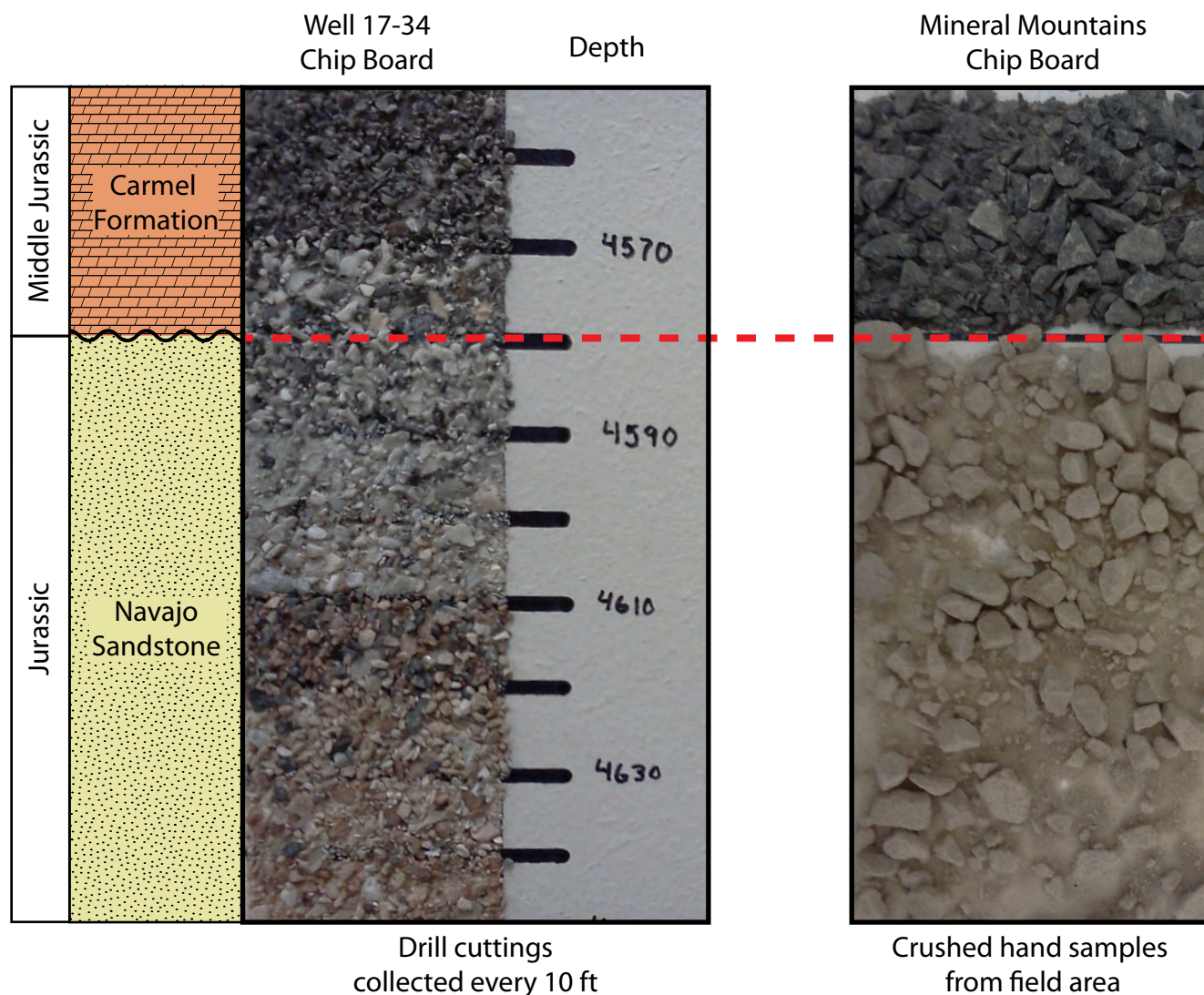


**Figure 11.** Example of a chip sample board for cuttings from borehole 17-34 and a board made by crushing a hand sample obtained from outcrop. These examples show chips from the Carmel Formation and Navajo Sandstone.

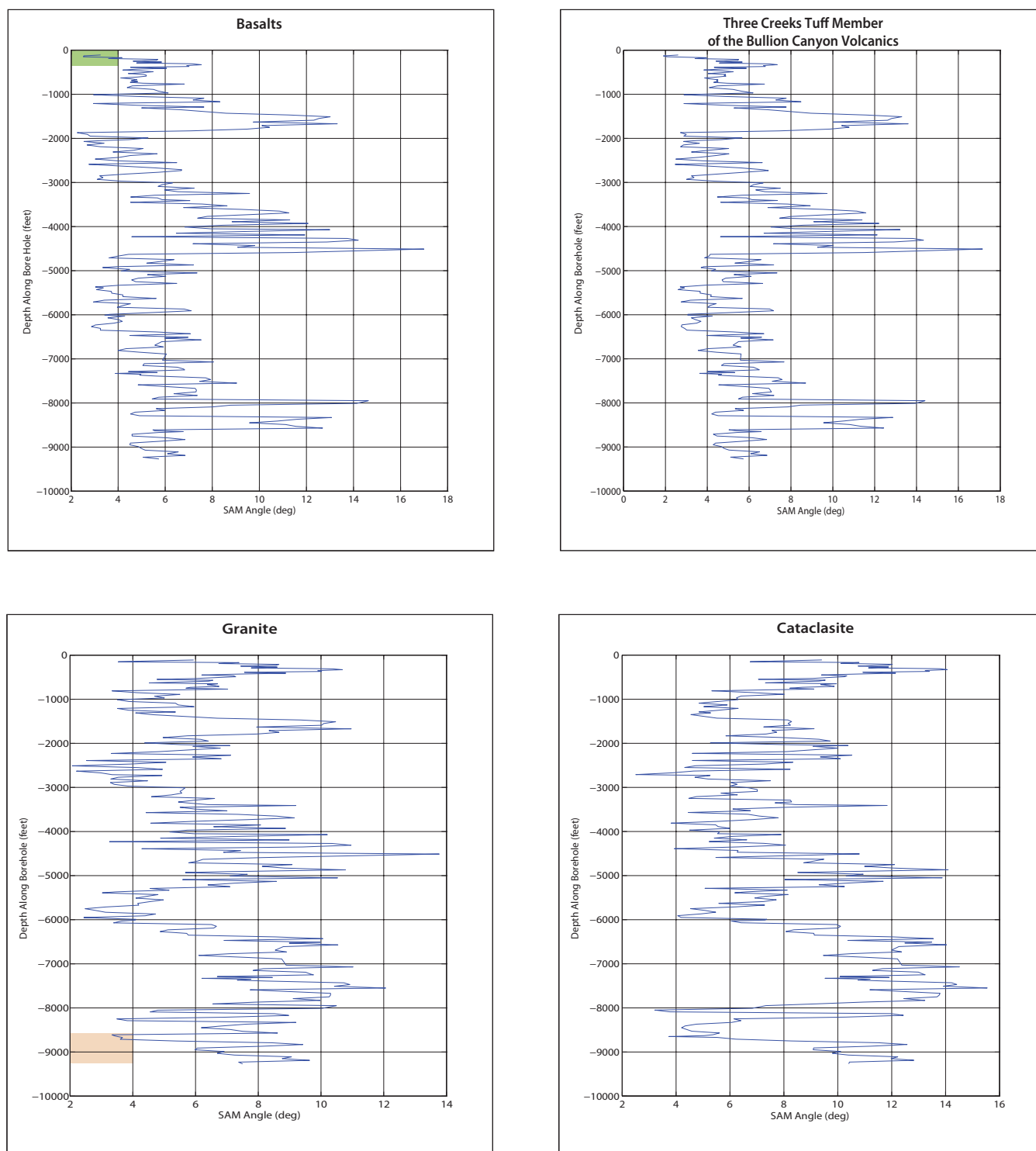


**Figure 12.** Rock type discrimination plots showing results of comparing the spectra of chip samples at various depths in well 17-34 with those of standards obtained from samples of outcrops in the Mineral Mountains. The vertical axis is depth measured along the well bore, and the horizontal axis is the angular miss-fit between the spectrum vectors of the well chip samples and the standard sample. The colored rectangles indicate the depth interval of the rock unit as interpreted from the well, and the width of each rectangle indicates the angular range within which the standard and well sample would theoretically match one another. This figure is discussed in detail in the text. Note that the figure contains plots for each individual unit (rock formation or type) that was analyzed.



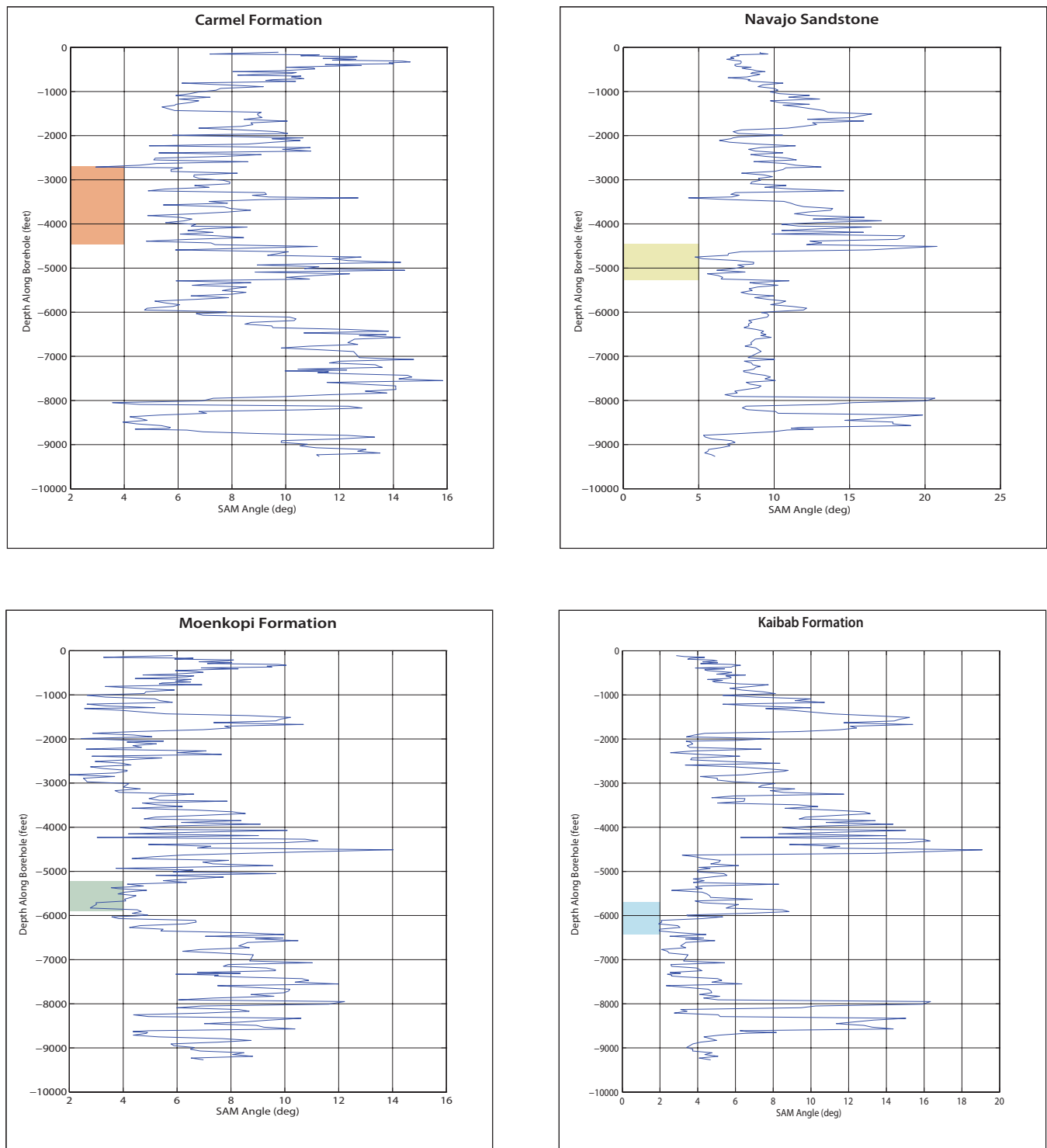
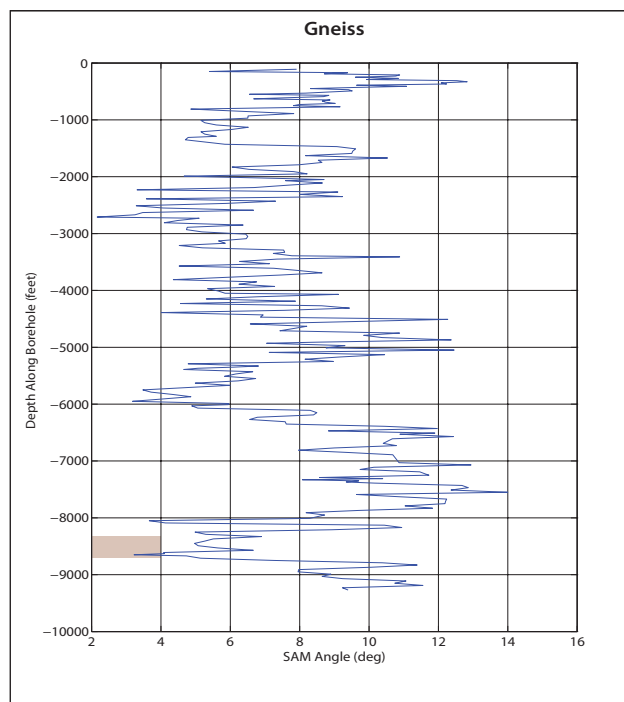
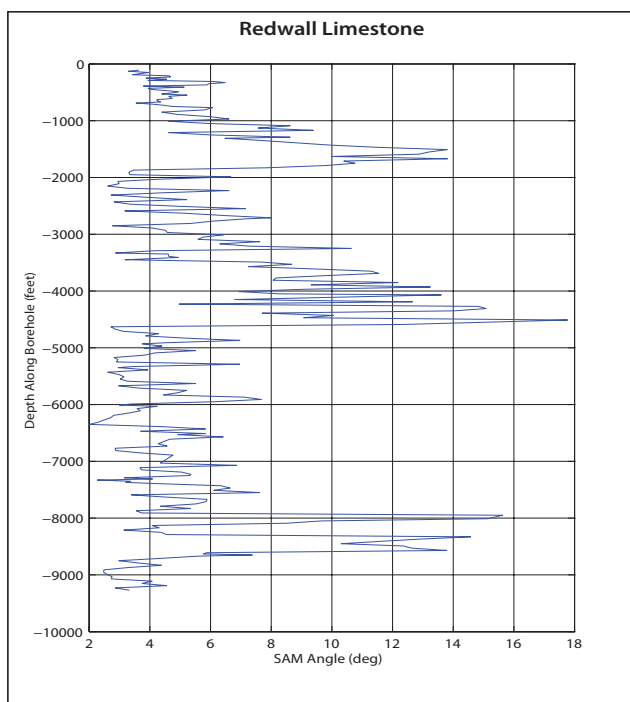
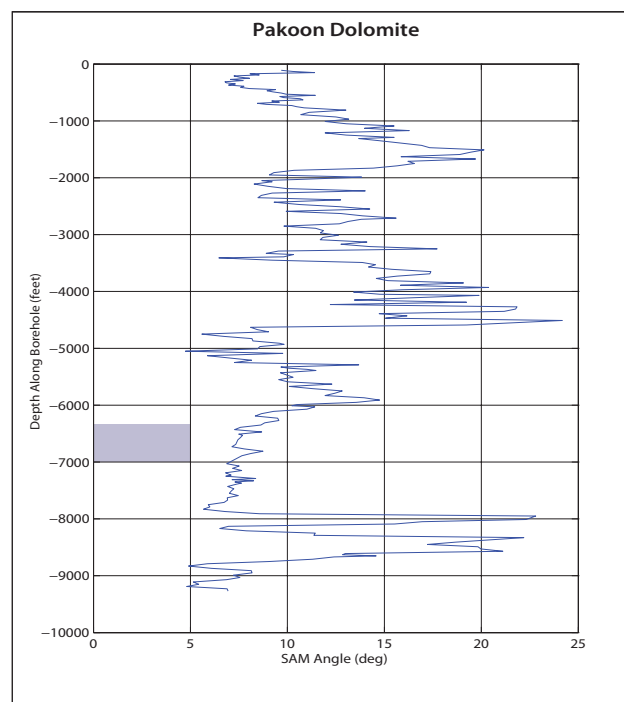
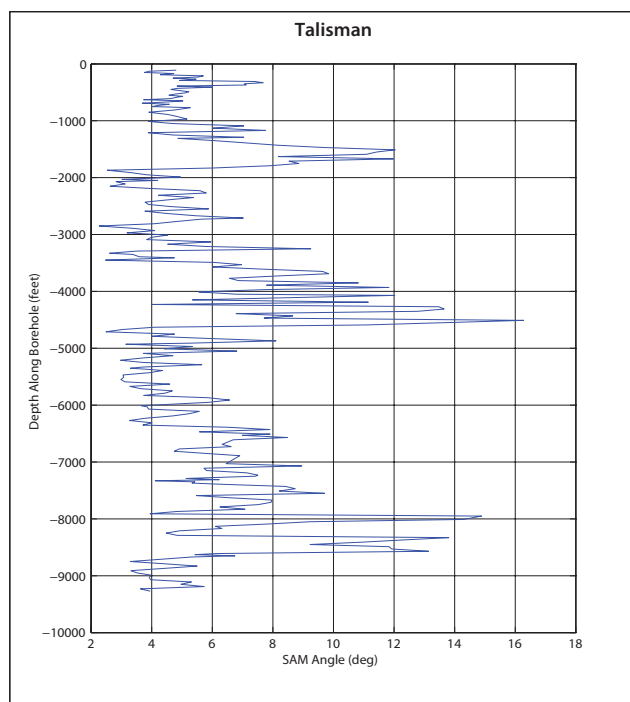


Figure 12. Continued.



**Figure 12.** *Continued.*

in southwestern Utah. Comminution of rocks during shearing along low-angle fault systems creates cataclasite that is susceptible to rapid sealing by hydrothermal alteration, unless breached by continued movement on the fault zone (Brown and Bruhn, 1996), or if high-angle faulting cuts and displaces the low-angle fault zone, breaching the relatively impermeable cataclasite.

There are several large detachment faults in southwestern Utah and adjacent parts of Nevada that are of interest to geothermal exploration geologists and geophysicists. These include the Cave Canyon detachment fault that we discuss in this report, the Sevier Desert detachment fault that dips westward beneath the northern part of the Sevier geothermal anomaly, and the Snake Range detachment that may extend beneath western Utah to intersect the Sevier Desert detachment at depth. Anders and others (2001) suggest that the Sevier Desert detachment may be a subsurface unconformity rather than a low-angle fault, but seismic reflection profiles would suggest that at least part of the feature is a fault that extends to mid-crustal depth. Lastly, Coleman and others (1997) cite evidence for a detachment fault with a break-away or “head” located on the eastern side of Beaver Valley. This latter fault is of great interest when evaluating the structural geology of the Thermo Hot Springs KGRA because it purportedly extends beneath the Mineral Mountains and contains the Cave Canyon detachment fault in its upper plate. Perhaps this fault contains the entire Thermo Hot Springs KGRA in its upper plate, including the granite and east-dipping detachment fault that we tentatively correlate with the Cave Canyon detachment. The existence of this cryptic “Beaver Valley” detachment is based primarily on evidence for uplift and back-rotation towards the east of the Mineral Mountains. Notably, the southern edge of one or both of the Beaver Valley and Cave Canyon detachment faults lies along the east-trending geomorphic escarpment that extends from the southern end of Beaver Valley almost continuously westward past the southern margin of the Thermo Hot Springs KGRA (figure 1).

Thrust faults may of course also be extensive barriers to upward migration of fluids because hydrothermal sealing of comminuted rock or cataclasite is likely. We note however, that thrust faulting within the Sevier orogenic belt of Utah was not accompanied by extensive volcanism or elevated heat flow. Conversely, development of detachment faults was accompanied by extensive plutonic and volcanic activity that elevated heat flow and generated hot fluids to enhance hydrothermal alteration and mineral sealing of the laterally extensive fault zones. While we would not exclude remnant thrust fault flats as important features for channeling lateral movement of subsurface fluids, we are particularly interested in the presence and permeability structure of the younger detachment faults that were associated with middle to late Tertiary volcanic activity.

## CONCLUSIONS

- We found no compelling evidence to support vertical stacking or duplication of the Mesozoic or Paleozoic section by thrust faulting based on our analysis of the stratigraphy penetrated in well 17-34.
- The structure and stratigraphy of well 17-34 is remarkably similar to that encountered in the central and southern Mineral Mountains, suggesting that the rocks and structures exposed in the Mineral Mountains provide a useful analog when discussing and evaluating the Thermo Hot Springs geothermal reservoir.
- Fossil fragments preserved in chip samples are useful in identifying the Carmel Formation, and determining that the Paleozoic rocks penetrated by well 17-34 are Mississippian and younger in age.
- We tentatively correlate the structural contact at the base of the Paleozoic section with the Cave Canyon detachment fault of the southern Mineral Mountains based on the presence of sheared “skarn”, metamorphic rocks and granite, extensive fracturing in the granite, and the hydrothermal alteration mineral assemblage.
- We suggest that the Cave Canyon detachment fault is offset by younger high-angle normal faults that also provide pathways for upwelling fluids. This conclusion is primarily the work of Nash and Jones (2010) who show vertical offset of the top of the granite in their cross sections of the KGRA.
- Further development of spectral surveying of outcrop and borehole chip samples to aid in correlation of subsurface stratigraphy is warranted, although the success in this study is modest at best.
- Additional study of large-scale detachment faults and blind geothermal reservoirs is certainly warranted given the structure of the Thermo Hot Springs KGRA and its intimate relationship to low-angle faulting between Paleozoic strata and underlying crystalline rocks.

## ACKNOWLEDGMENTS

This work represents part of the M.S. thesis (in progress) of Mr. Warren Anderson at the University of Utah, Department of Geology and Geophysics. We especially thank Dr. Joseph Moore and Mr. Clay Jones of the Energy and Geosciences Institute at the University of Utah for their help in obtaining data and the exchange of ideas. Dr. Moore spent hours with

Mr. Anderson reviewing petrographic sections from Thermo Hot Springs and teaching him how to identify minerals. Dr. Moore also made many valuable comments concerning the geology. Dr. Rick Allis of the Utah Geological Survey originally put forward the idea that low-angle faulting was perhaps a key feature in development of the Sevier geothermal anomaly. Although we have not tackled that problem “head on” in this research his idea did motivate us in our work on the Thermo Hot Springs KGRA. The Utah Geological Survey supported the research through an energy and minerals research grant, with funds partially supplemented by Raser Technologies, Inc.

## REFERENCES

- Anders, M.H., Christie-Blick, N., and Wills, S., 2001, Rock deformation studies in the Mineral Mountains and Sevier Desert of west-central Utah: Implications for upper crustal low-angle normal faulting: Geological Society of America Bulletin, v. 113, p. 895–107.
- Barnett, D.E., Bowman, J.R., Bromley, C., and Cady, C., 1996, Kinetically limited isotope exchange in a shallow level normal fault, Mineral Mountains, Utah: Journal of Geophysical Research, v. 101, p. 673–685.
- Brown, S.R., and Bruhn, R.L., 1996, Formation of voids and veins during faulting: Journal of Structural Geology, v. 18, p. 657–661.
- Bruhn, R.L., Parry, W.T., Yonkee, W.A., and Thompson, T., 1994, Fracturing and hydrothermal alteration in normal fault zones: Pure and Applied Geophysics, v. 142, p. 609–644.
- Bruhn, R.L., Yusas, M.R., and Huertas, F., 1982, Mechanics of low-angle normal faulting: An example from Roosevelt Hot Springs geothermal area, Utah: Tectonophysics, v. 86, p. 343–361.
- Charette, E.K., 1998, Taphonomy and paleoecology of a Middle Jurassic fossil assemblage, Carmel Formation, southwest Utah: <http://keckgeology.org/files/pdf/symvol/11th/Utah/charette.pdf>
- Cheevers, C.W., and Rawson, R.R., 1979, Facies analysis of the Kaibab Formation in northern Arizona, southern Utah, and southern Nevada: Four Corners Geological Society Guidebook, Ninth Field Conference, p. 105–113.
- Coleman, D.S., Bartley, J.M., Walker, J.D., Price, D.E., and Friedrich, A.M., 1997, Extensional faulting, footwall deformation and plutonism in the Mineral Mountains, southern Sevier Desert, in Link, P.K., and Kowallis, B.J., editors, Mesozoic to recent geology of Utah: Brigham Young University Geology Studies, v. 42, part 2, p. 203–233.
- Cowan, D.S., and Bruhn, R.L. 1992, Late Jurassic to early Late Cretaceous Geology of the U.S. Cordillera (in) The cordilleran orogen: coterminous U.S. *Volume G-3 Decade of North American Geology* (DNAG), Geological Society of America, Boulder Co., 1992, p. 169–204.
- De Gibert, J.M., and Ekdale, A.A., 1999, Trace fossil assemblages reflecting stressed environments in the Middle Jurassic Carmel Seaway of Central Utah: Journal of Paleontology, v. 73, p. 711–720.
- Huttrer, G., 1994, Geothermal exploration at Cove Fort–Sulphurdale, Utah, 1972–1992, in Blackett, R.E., and Moore, J.N. editors, 1994, Cenozoic Geology and Geothermal Systems of Southwestern Utah: Utah Geological Association Publication 23, p. 61–68.
- Kruse, F.A., Lefkoff, A.B., Boardman, J.B., Heidebrecht, K.B., Shapiro, A.T., Barloon, P.J., and Goetz, A.F.H., 1993, The Spectral Image Processing System (SIPS) Interactive Visualization and Analysis of Imaging spectrometer Data: Remote Sensing of the Environment, v. 44, p. 145–163.
- Marshak, S., Mitra, G., 1988, Basic Methods of Structural Geology, Englewood Cliffs, NJ: Prentice Hall, 253 p.
- Mabey, D.R., and Budding, K.E., 1987, High-temperature geothermal resources of Utah: Utah Geological and Mineral Survey Special Studies 123, 64 p.
- Mabey, D.R., and Budding, K.E., 1994, Geothermal resources of southwestern Utah, in Blackett, R.E., and Moore, J.N. editors, 1994, Cenozoic Geology and Geothermal Systems of Southwestern Utah: Utah Geological Association Publication 23, p. 1–25.
- Moore, J.N., Ross, H.P., Nash, G.D., and Barker, B., 2009, The geology, geophysics and geochemistry of the Thermo Hot Springs Area, Utah, with an emphasis on Raser Technologies Well 21-24: Energy and Geosciences Institute, University of Utah, unpublished report, 19 p.
- Nash, G.D., and Jones, C., 2010, Thermo Geothermal Drilling Program Rock Reports: Wells 11-34, 24-34, 13-34A, 58-34, 52-34, 21A-34, 63-33, 74-34, and 17-34: Energy and Geosciences Institute, University of Utah, unpublished report, 56 p.
- Nielson, D.L., Evans, S.H., Jr., and Sibbett, B.S., 1986, Magmatic, Structural, and Hydrothermal Evolution of the Mineral Mountains Intrusive Complex, Utah: Geological Society of America Bulletin, v. 97, p. 765–777.
- Ross, H., and Moore, J.N., 1994, Geophysical investigations of the Cove Fort–Sulphurdale geothermal system, Utah, in Blackett, R.E., and Moore, J.N. editors, 1994, Cenozoic Geology and Geothermal Systems of Southwestern Utah: Utah Geological Association Publication 23, p. 45–60.
- Rowley, P.D., 1978, Geologic map of the Thermo 15-minute quadrangle, Beaver and Iron Counties, Utah, U.S. Geological Survey Map GQ-1493.
- Rowley, P.D., Lipman, P.W., Mehnert, H.H., Lindsey, D.A., and Anderson, J.J., 1978, Blue Ribbon Lineament, an east-trending structural zone within the Pioche Mineral Belt of southwestern Utah and eastern Nevada: U. S. Geological



- Survey Journal Research, v. 6, no. 2, p. 175–192.
- Rowley, P.D., Vice, G.S., McDonald, R.E., Anderson, J.J., Machette, M.N., Maxwell, D.J., Ekren, B.E., Cunningham, C.G., Steve, T.A., and Wardlaw, B.R., 2005, Interim Geologic Map of the Beaver 30' x 60' Quadrangle, Beaver, Piute, Iron, and Garfield Counties, Utah: Utah Geological Survey Open-File Report 454, 29 p., 1 plate, scale 1:100,000.
- Sawyer, R.F., 1977, Gravity and ground magnetic surveys of the Thermo Hot Springs KGRA region, Beaver County, Utah: Salt Lake City, University of Utah, Department of Geology and Geophysics, M.S. thesis, v. 77-6, 42 p.
- Schubert, J.K., and Bottjer, D.J., 1995, Aftermath of Permian-Triassic extinction event: Paleoecology of Lower Triassic carbonates in the western USA: *Palaeogeography, Palaeoclimatology, Palaeoecology*, v. 116, p. 1–39.
- Smith, R.B., and Bruhn, R.L., 1984, Intraplate extensional tectonics of the eastern Basin-Range: Inferences on structural style from seismic reflection data, regional tectonics, and thermal-mechanical models of brittle-ductile deformation: *Journal of Geophysical Research*, v. 89, p. 5733–5762.
- Steven, T.A., Morris, H.T., and Rowley, P.D., 1990, Geologic map of the Richfield 1 x 2 degree Quadrangle, Utah: U.S. Geological Survey Miscellaneous Investigations Series Map I-1901, 1 plate, scale 1:250,000.